# Differentiation of hPSC derived embryoid bodies to atrial and ventricular cardiomyocytes in a trapping system on a chip

Defining requirements towards asymmetric differentiation

B.A.M. Wesselink

August 30, 2022

Master's Thesis

Britt Wesselink

Master Biomedical Engineering
Track: Bioengineering Technologies

Graduation Committee:

| | |
|---|---|
| Dr. A.D. van der Meer | Applied Stem Cell Technologies, University of Twente |
| Dr. A.R Vollertsen | Applied Stem Cell Technologies, University of Twente |
| Prof. Dr. Ir. M. Odijk | BIOS Lab-on-a-Chip group, University of Twente |

Daily supervisors:

| | |
|---|---|
| Simone ten Den | Applied Stem Cell Technologies, University of Twente |
| Dr. V. Schwach | Applied Stem Cell Technologies, University of Twente |

Department of Applied Stem Cell Technologies

Techmed Centre
Faculty of Science and Technology
University of Twente

August 30, 2022


UNIVERSITY OF TWENTE. | TECHMED CENTRE

UNIVERSITY OF TWENTE

# *Abstract*

Faculty of Science and Technology

Master of Science

**Differentiation of hPSC derived embryoid bodies to atrial and ventricular CMs in a trapping system on a chip; Defining requirements for asymetric differentiation on chip**

by BRITT WESSELINK

Human pluripotent stem cells (hPSCs)-derived cardiomyocytes (CMs) have an advantage in studying regenerative medicine, disease modeling, drug screening, and early cardiomyogenesis. Ideal platforms should consist of both atrial and ventricular tissues due to the unique chamber-specific defects and drug-induced myopathies present in the atria and ventricles. BMS-753 is an essential signaling molecule in the differentiation of hPSCs towards atrial cardiomyocytes. Traditional culture plates make it impossible to asymmetrically differentiate atrial cardiomyocytes (AMs) and ventricular cardiomyocytes (VMs) due to diffusion of this signaling molecule.

The main goal of this project is to determine the biological limitations of moving the embryoid body (EB) differentiation from standard well plate culture to a microfluidic device which can in future enable asymmetric differentiation to AMs and VMs. First, replication of the RAR-$\alpha$ Schwach et al.'s protocol was performed to rule out systematic errors. By performing flow cytometry analysis the generated AMs and VMs were characterized for determining the percentage of NKX2.5$^{eGFP}$ and COUP-TFII$^{mCherry}$ and fluorescence imaging is done to examine the NKX2.5$^{eGFP}$ and COUP-TFII$^{mCherry}$ expression. Based on the results, the following observations were made in regard to asymmetric differentiation on a chip. The student LAF in ML-1 is not suited for EB differentiation. A better alternative is the BIC ML-2 lab because pipettes are better calibrated and incubators are more stable. Second, EB growth over time using different initial cell seeding densities was measured. Cell seeding density does not have a lot of impact on the EB size, while it does have an influence on the percentages of VMs and AMs. Third, the transition in AM and VM induction using different BMS concentrations was tested. A mixed population is obtained using 0.5 and 1 $\mu$M BMS. Finally, three chip designs were designed, fabricated and tested by culturing EBs in the device. The trapping systems shown here partially worked for hPSCs differentiation towards VMs as could be seen by the proof-of-concept.

All in all, some requirements were defined for differentiation of hPSCs derived EBs towards asymmetric differentiation of AMs and VMs in a microfluidic system. For the future, a model is presented that should be able to maintain a gradient of BMS-753 while trapping an embryoid body.

## Samenvatting - Nederlands

Van menselijke pluripotente stamcellen afgeleide cardiomyocyten kunnen een representatief model vormen voor het bestuderen van regeneratieve geneeskunde, ziektemodellering, screening van geneesmiddelen en vroege cardiomyogenese. Ideale platforms moeten bestaan uit zowel atriale als ventriculaire weefsels vanwege de unieke kamerspecifieke defecten en door geneesmiddelen geïnduceerde myopathieën die aanwezig zijn in de atria en ventrikels. BMS-753 is een essentieel signaalmolecuul bij de differentiatie van hPSC's naar atriale cardiomyocyten. Traditionele kweekplaten maken het onmogelijk om AM's en VM's asymmetrisch te differentiëren vanwege diffusie van dit signaalmolecuul.

Het belangrijkste doel van dit project is om de biologische beperkingen te bepalen van het verplaatsen van de EB-differentiatie van een standaard putplaatcultuur naar een microfluïdisch apparaat dat in de toekomst asymmetrische differentiatie naar AM's en VM's mogelijk kan maken. Ten eerste werd replicatie van het RAR-alpha-protocol van Schwach et al. uitgevoerd om systematische fouten uit te sluiten. Door flowcytometrie-analyse uit te voeren, werden de gegenereerde AM's en VM's gekarakteriseerd voor het bepalen van het percentage NKX2.5$^{eGFP}$ en COUP-TFII$^{mCherry}$ en werd fluorescentiebeeldvorming uitgevoerd om de NKX2.5$^{eGFP}$ en COUP-TFII$^{mCherry}$ expressie te onderzoeken. Op basis van de resultaten zijn de volgende observaties gedaan. De student LAF in ML-1 is niet geschikt voor EB differentiatie. Een beter alternatief is het BIC ML-2 lab omdat pipetten beter gekalibreerd zijn en incubators stabieler zijn. Ten tweede werd EB-groei in de loop van de tijd gemeten met behulp van verschillende initiële celzaaidichtheden. Cell seeding density heeft niet veel invloed op de EB-grootte, terwijl het wel invloed heeft op de percentages VM's en AM's. Ten derde werd de overgang in AM- en VM-inductie met verschillende BMS-concentraties getest. Een gemengde populatie wordt verkregen door gebruik te maken van 0,5 en 1 $\mu$M BMS. Ten slotte werden drie chipontwerpen ontworpen, gefabriceerd en getest door EB's in deze systemen te kweken. De hier getoonde trapping-systemen werkten gedeeltelijk voor hPSC-differentiatie naar VM's, zoals blijkt uit de proof-of-concept.

Al met al werden enkele vereisten gedefinieerd voor differentiatie van van hPSC's afgeleide EB's naar asymmetrische differentiatie van AM's en VM's in een microfluïdisch systeem. Voor de toekomst wordt een model gepresenteerd dat in staat zou moeten zijn om een gradiënt van BMS-753 te behouden terwijl een embryoid lichaam wordt gevangen.

# *Acknowledgements*

During this final period of my Master, I have learned so much about how to independently perform research and how to overcome obstacles and achieve milestones. I could not have undertaken this journey without a few people, who generously provided knowledge and expertise.

Special acknowledgements go out to my daily supervisor Dr. Anke Vollertsen for her expertise and support on a daily basis during my Master Thesis. We know each other for already four years and in those years I got very inspired and motivated by her as a person and her work and achievements. I am very grateful that I was able to learn from and work with such a specialized person. Furthermore, I would like to thank Simone ten Den for daily assistance during my stem cell differentiation experiments and to help me upgrade my work quicker to a higher level. The different knowledge of Anke and Simone helped me to push my research in the right direction.

I wish to extend my special thanks to Dr. Andries van der Meer as head of my committee. His open mindset and constructive feedback helped me find my own way of performing research. His door was always open to ask questions or just to listen. Great thanks to Prof. Dr. Ir. Mathieu Odijk as external supervisor. His different look and knowledge of organs-on-chips and microfluidics helped significantly in chip designs and fabrication.

Additionally, the work of this thesis was dominated with work on atrial and ventricular differentiation of human pluripotent stem cells, which would not have been possible without the knowledge of Dr. Verena Schwach and the help of Carla Cofiño Fabres. Many thanks to them. Moreover, I would like to thank Kim Vermeul for her technical support and Tarek Gensheimer for providing a helping hand by micro-mill simulations.

Many thanks to the whole AST team who made me feel very welcome and who provided the nice lunch breaks, motivational presentations, and enjoyable group activities. I am thankful for all the interesting conversations and advice I have received from the multiplexed and automation meetings and the organ-on-chip meetings. I also want to thank all the students from the student table for their assistance, laughter, and occasionally complaints.

Finally, I am also grateful to fellow students Meike Große-Elshoff and Sabine de Winter for being my project buddies to support me and give me new insights into the study.

# Contents

# List of Abbreviations

| | |
|---|---|
| **2D** | **t**wo **d**imensional |
| **3D** | **t**hree **d**imensional |
| **ACD** | **a**symmetric **c**ell **d**ivision |
| **AM** | **a**trial **c**ardiomyocyte |
| **AST** | **a**pplied **s**tem cell **t**echnologies |
| **AV** | **a**trio**v**entricular node |
| **BMP** | **b**one **m**orphogenetic **p**rotein |
| **BMS-753** | 4-[[(2,3-Dihydro-1,1,3,3-tetramethyl-2-oxo-1H-inden-5-yl)-carbonyl]amino]-benzoic acid |
| **BPEL** | **b**ovine serum albumin (BSA) **p**olyvinylalcohol **e**ssential **l**ipids |
| **CAD** | **c**omputer **a**ided **d**esign |
| **CAM** | **c**omputer **a**ided **m**illing |
| **CM** | **c**ardio**m**yocyte |
| **CPC** | **c**ardiac **p**rogenitor **c**ell |
| **COUP-TFII** | **c**hick **o**valbumin **u**pstream **p**romoter **t**ranscription **f**actor **II** |
| **CVD** | **c**ardio**v**ascular **d**isease |
| **EB** | **e**mbryoid **b**ody |
| **EHT** | **e**ngineered **h**eart **t**issue |
| **GF** | **g**rowth **f**actor |
| **GFP** | **g**reen **f**luorescent **p**rotein |
| **hESC** | **h**uman **e**mbryonic **s**tem **c**ell |
| **hPSC** | **h**uman **p**luripotent **s**tem **c**ell |
| **iPSC** | **i**nduced **p**luripotent **s**tem **c**ell |
| **LoC** | **l**ab-**o**n-a-**c**hip |
| **mLSI** | **m**icrofluidic **l**arge-**s**cale **i**ntegration |
| **mCherry** | **m**onomeric **Cherry** |
| **NKX2.5** | **NK2** Homeobo**x 5** |
| **OoC** | **o**rgan-**o**n-**c**hip |
| **PDMS** | **p**oly**d**i**m**ethyl**s**iloxane |
| **PEB** | **p**rotein **e**xtraction **b**uffer |
| **PMMA** | **p**oly**m**ethyl **m**eth**a**crylate |
| **PMV** | **p**neumatic **m**embrane **v**alve |
| **PVA** | **p**oly (**v**inyl **a**lcohol) |
| **RAR$\alpha$** | **r**etinoic **a**cid **r**eceptor **a**lpha |
| **RFP** | **r**ed **f**luorescent **p**rotein |
| **rpm** | **r**ounds **p**er **m**inute |
| **SA** | **s**i**n**oatrial node |
| **SCD** | **s**ymmetric **c**ell **d**ivision |

| | |
|---|---|
| **SCF** | **s**tem **c**ell **f**actor |
| **VEGF** | **v**ascular **e**ndothelial **g**rowth **f**actor |
| **VM** | **v**entricular **c**ardiomyocyte |
| **Wnt** | **w**ingless-related i**nt**egration |

# 1 | Introduction

## 1.1 The importance of combining cardiomyocyte subtypes

Cardiovascular diseases have a huge impact on the humans health and causes rising health care costs [1, 2]. It is a general term for conditions affecting the heart or blood vessels [3]. Understanding the developmental stages that a structure or region goes through during its embryogenesis provides crucial hints regarding both the region's typical structure and the causes of anatomical variance [4]. Embryogenesis which is defined by a sequential series of dynamic processes that include cell division enlargement and differentiation. The cardiovascular system's embryological development begins with heart.

The heart is the most essential muscle in the human body which pumps 5-6 liters of blood per minute throughout the body by contraction to distribute oxygen, nutrients, hormones, and warmth. Several muscle layers, chambers (two atria and two ventricles), valves, and nodes work together (figure 1.1) [5]. The upper two chambers are the atria. It receives blood from the body and contracts to move the blood towards the ventricles. A ventricle is one of the larger bottom chambers in the heart that receives blood from the atria and pumps blood towards the body.

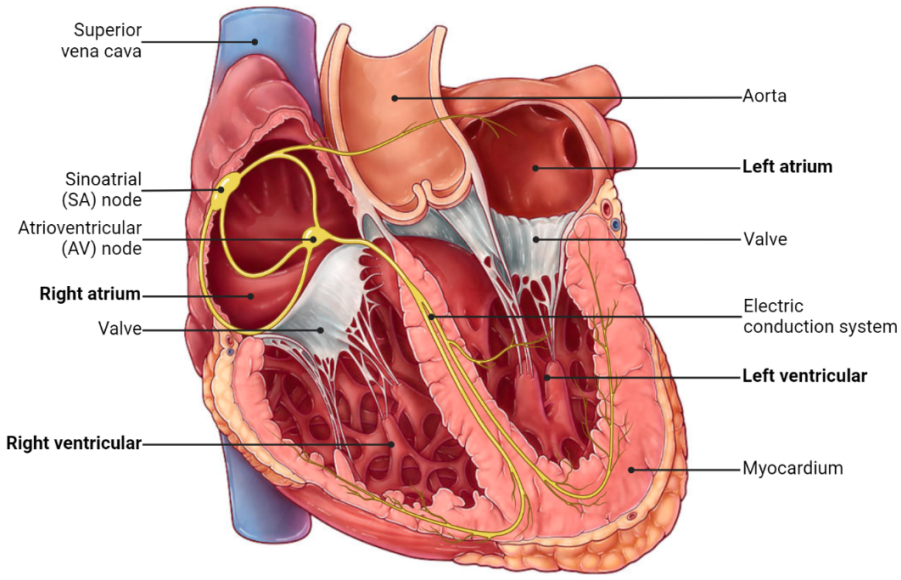


FIGURE 1.1: The human heart with all chambers and the electrical conduction system. Created in Biorender.

Cardiac muscle cells, also known as cardiomyocytes (CMs) form the middle muscle layer, called the myocardium which are the most abundant cell type in the heart and are responsible for the contraction of the heart. The majority (99%) of the cells in the atrium and

ventricles known as the atrial and ventricular CMs, are myocardial contractile cells [6]. The other one percent form the conduction system of the heart.

Understanding the roles and interplay of both atrial and ventricular CMs can help understanding embryogenesis and thus how organs form. The most basic principles can give insight into abnormal development or diseases [4]. Animal models can help progress on the general understanding of the biological and physiological processes, but often fail to exactly represent human cardiotoxicity due to inter-species differences [7]. It has severe drawbacks such as time, money, and resource consuming and is ethically controversial [8]. Other non-human *in vitro* models have lack of predictivity and cannot be directly compared to the human body, which are major reasons for an inefficient process [9–11]. This problematic situation has instigated research using human-induced pluripotent stem cells (control or patient-derived) for disease modeling, drug discovery, and regenerative medicine. hPSCs have the capability to differentiate into all cells of the human body, including various CM subtypes of the heart, like with embryogenesis.

## 1.2 Cardiomyocyte subtypes

### 1.2.1 Differentiation of hPSCs to VMs and AMs

Human primary CMs for *in vitro* three-dimensional (3D) culture are difficult to obtain and do not proliferate. As a solution, stem cell-derived CMs have advantage in studying regenerative medicine, disease modelling, drug screening and early cardiomyogenesis [12–16]. Most approaches for disease modeling and drug testing during the last decade have focused on ventricular myocardium and derived from HPSCs [13, 17–28].

Induction of the atrial or ventricular phenotype can be performed by manipulation of the bone morphogenetic protein (BMP), activin-nodal, wingless-related integration (Wnt), and retinoic-acid (RA) signaling pathways [14, 29, 30]. An optimized protocol for the generation of AMs and VMs by modulating the RA signaling cascade during differentiation of hPSCs is previously described by Schwach et al. [31]. The main differences in atrial versus ventricular differentiation protocols is that the addition of RA selectively induces the retinoic acid receptor alpha (RAR$\alpha$) to induce differentiation of atrial cardiomyocytes. By alternating this RA signaling pathway at the mesodermal stage of hPSC differentiation, it was shown that AMs and VMs develop from distinct cardiac mesoderm progenitors [32]. Optimization of the atrial differentiation protocol by administration of the RAR$\alpha$ selective agonist BMS-753 showed improved atrial differentiation of hPSCs [33].

### 1.2.2 Unique properties of VMs and AMs

Human ventricular myocardium is a poor model for the development of discovery of atrial drugs due to the unique chamber-specific defects and drug-induced myopathies present in the atria and ventricles [34]. Especially, atrial-specific platforms are important for cardiac arrhythmia, since drugs treating this irregular heartbeat have fatal unwanted side-effects on VMs [35–39].

The cellular and molecular mechanisms responsible for the separation of ventricular and atrial lineages are still not well-understood [40]. Other cell types such as pacemaker cells and other myocardial conducting cells are also involved in the structure of the heart. When looking at the contraction of the heart, it is not just from one AM to another ventricular cardiomyocyte VM but more complex. Contraction is caused by the electrical conduction system of the heart that transmits signals produced by the sinoatrial (SA) node to the heart muscle, via the atria to the atrioventricular (AV) node to the ventricles (figure 1.1) [6].

### 1.2.3 Combining VMs and AMs in microfluidic system

During the last decade, several studies have focused on hPSCs derived VMs [13, 17]. Only recently, AMs are also used in cardiac disease modeling [30, 32, 41, 42] and drug-induced research [43, 44]. Ideal platforms should consist of both atrial and ventricular tissues, given that AMs and VMs have distinct properties [45]. Combining the differentiation of both VMs and AMs would give more insight in the embryogenesis process. When such information is combined with knowledge of when and where specific structural abnormalities begin during embryogenesis, therapeutics can facilitate better understanding of underlying disease mechanisms as well as drug development [4].

Both differentiation of to human AMs and VMs from hPSCs has been decribed previously [33]. By adding different concentrations of differentiation factors, the CMs can be pushed more towards atrial or ventricular subtypes. Recently it is shown that cardiomyocytes can be differentiated from hPSCs by spontaneous differentiation of 3D cell aggregates called embryoid body (EB) in suspension, and guiding the cardiac differentiation with defined growth factors [33, 46].

Strategies for asymmetric cell differentiation into localized groups of subtypes directly within the heart model would be advantageous. Asymmetric cell division (ACD) results in the development of two daughter cells with different fates after a single mitosis (Figure 1.2b) [47–49]. Alternatively, stem cells can undergo proliferating symmetric cell divisions (SCD) which give rise to two daughter with the same fates (Figure 1.2) [47]. A balance between these two forms of division is necessary for normal development and homeostasis.

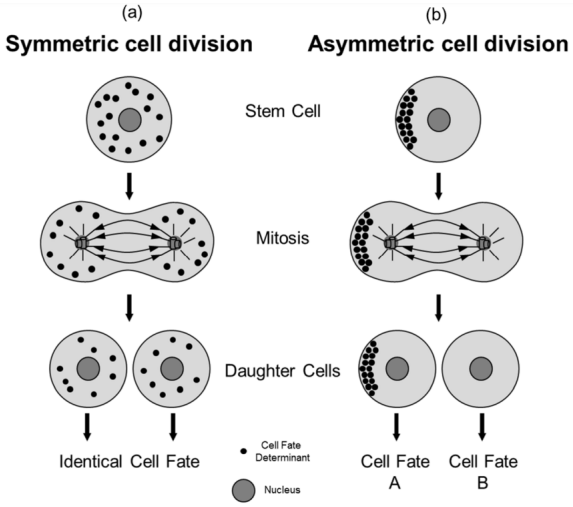


FIGURE 1.2: Symmetric versus Asymmetric Cell Division. During a SCD (a), cell fate determining factors are distributed evenly to both arising daughter cells, resulting in identical cell fates. During ACD (b) cell fate determinants segregate unequally into both daughter cells, enabling them to realize different cell fates [47].

ACD can be established through exposure to cell extrinsic signaling cues. As a result, asymmetric distribution of so-called cell fate determinants, e.g., membrane components, cell organelles, cytosolic components or proteins is received. As described, cardiac subtypes such as AMs and VMs can be produced by altering the RA signaling pathway by adding either the RAR$\alpha$ selective agonist BMS-753 or not. By using a biological gradient of this selective agonist, ACD can be established. Gradients created by the secretion or metabolism

of morphogens enable complex patterning [50]. Without these gradients, cells cease to function and complex organisms would not develop. Microplates have become a standard tool for analytical research and clinical diagnostic testing laboratories, but are limited in creating gradients due to mass transport. As the main goal is to set up requirements to enable asymmetric differentiation, this is important to notice.

## 1.3 Current models for 3D culture on microfluidic devices

Over the last decades several microfluidic devices have been developed that enable the generation of 3D aggregates. Furthermore, it is possible to control flow in microfluidic devices to create gradients [51, 52].

A simple chip system that is able to place and grow a spheroid consists of a U-shaped well (figure 1.3A) [53]. This design enables constant perfusion and dynamic drug concentrations (see figure 1.3A). On-chip growth was shown to be comparable with the *in vivo* situation. Nevertheless, this system is not able to have a gradient since it has the same shape as a U-shaped wells plate.

Other studies show perfusable devices based on SU-8 lithography and polydimethylsiloxane (PDMS) for culturing aggregated spheroids [54–56]. However, these techniques using pneumatic micropumps fail to regulate oxygen levels due to minimal gradients as required for EB culturing and differentiation. Oxygen gradients are necessary to create and keep oxygen homeostasis after early embryonic morphogenesis and later in development. This enables the organism to sustain oxygen gradients and keep oxygen levels within the acceptable range for growth. To create even oxygen levels through the whole system several approaches are already used. These approaches can broadly be classified in two main categories: on one hand, engineering approaches implemented at the device level during its fabrication, e.g., through proper choice of materials employed to build the microfluidic device. On the other hand, most approaches to control oxygen in microfluidic devices focus on the type of material. Open wells or permeable materials allow oxygen to permeate through [57].

Khoury et al. developed a device which could create 3D aggregates in prolonged culture with optimized conditions (figure 1.3B) [58]. Note that staining efficiency decreased towards the back of the trap due to its diffusion limited nature, however no dead cells are present, as the oxygen levels were sufficient. The traps have a unique U-shaped design to promote cell capture and aggregation while providing efficient gas/nutrients exchange. EBs developed and differentiated and showed viability for more than 5 days. Other examples of such cell trapping mechanism using flow-through obstacles are shown by Luan et al. [59] who shows different trapping shapes, such as polygonal, U-shaped, and butterfly shaped geometries.

Automated microfluidics has also been shown to be compatible with stem cell differentiation (towards cardiomyocytes) and can be used for screening a wide variety of conditions [60, 61]. However, most of these systems were designed for 2D cell culture under uniform conditions. Instead, Ardila Riveros et al. developed a microfluidic large-scale integration (mLSI) chip platform for combined automated 3D cell culturing and high-throughput imaging (figure 1.3C) [62]. Such system makes use of micromechanical valves that can be independently operated. Those valves are created by multilayer soft lithography where at least two independently addressable microfluidic layers, often called flow and control layer, are bound to each other. A valve can be either open, restricted or closed due to increasing pressure in the control layer. In such a way, the EB is protected from direct shear flow and the membrane can retract to provide more space when the EB is growing. A schematic representation of their system is displayed in Figure 1.3C.

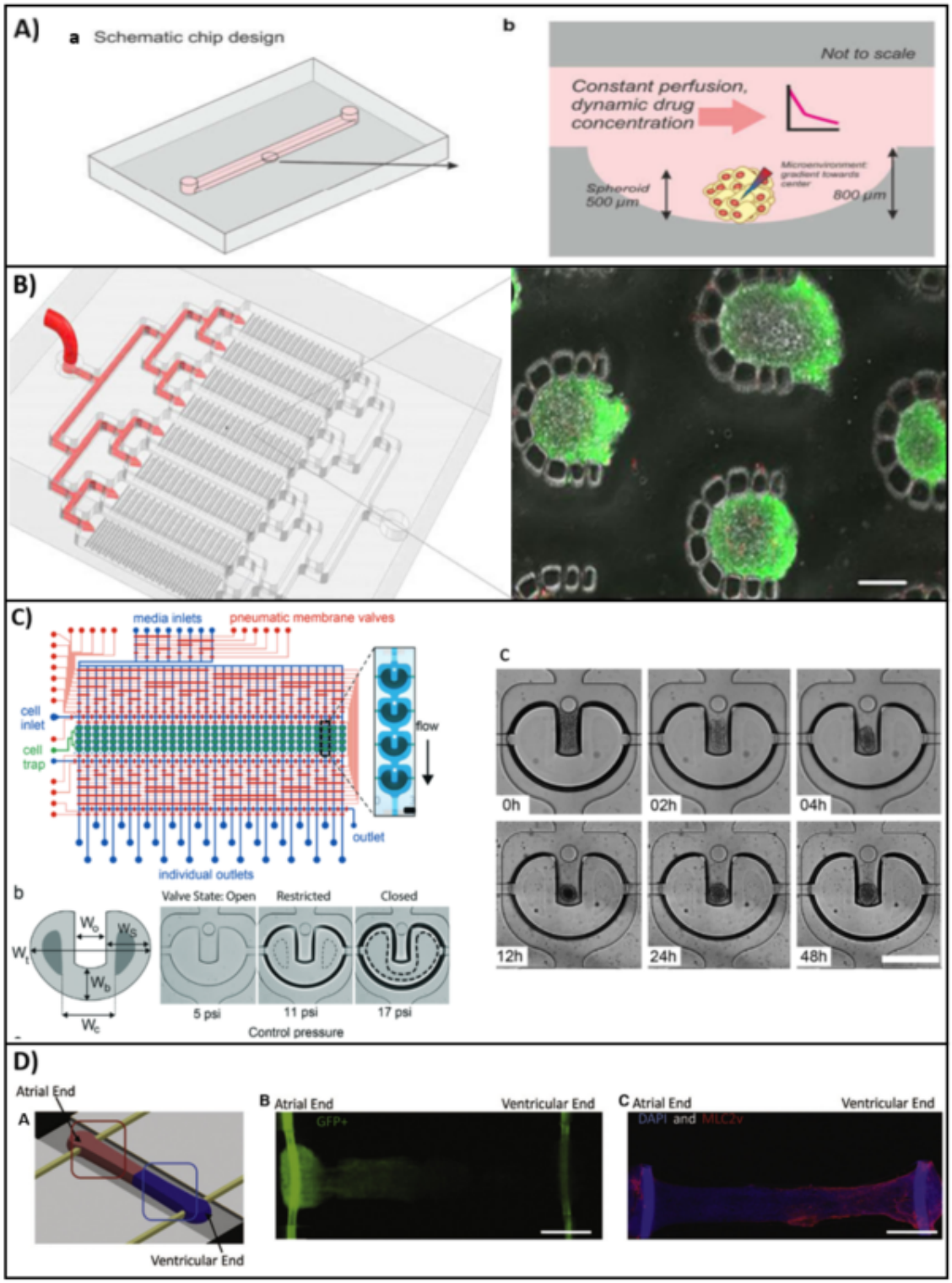


FIGURE 1.3: **A)** Schematic two part chip design consisting of a 21 × 2 × 1 mm (l × w × h) top channel for continuous perfusion and dynamic drug concentrations and a U-shaped well for spheroid placement and growth by Carvalho et al. [53]. **B)** Microfluidic device of Khoury et al. [58] in segmented microtraps. Live cells are stained green and dead cells are stained red. (Scale bar: 100 $\mu$m) **C)** Microfluidic large-scale integration chip platform of Ardila Riveros et al. [62] for hiPSC culturing and differentiation. (Scale bar: 500 $\mu$m) **D)** A scalable cardiac tissue cultivation platform enables assessment of multiple parameters of atrial and ventricular tissue function, drug testing, and disease modeling by Zhao et al. [63]. (Scale bar: 0.5 mm).

## 1.4 Current models for multiple cell sources

Next to models for 3D culture, studies have also focused on heart models [64–67]. Despite hPSCs-derived heart models developing fast, there exist only a few models consisting of multiple cell sources. Research is still mostly focused on generating ventricular tissues such as construct called the I-wire or Biowire for generating three-dimensional engineered heart tissues (EHTs) from hPSC-CMs [24, 68].

For example, Abulaiti et al. [69] exploits a novel system consisting of dynamic culture-based 3D iPSCs-derived cardiac microtissues consisting of a mixture of cells. However, the generation of those microtissues is very extensive due to the many handling steps. Another study focused on developing a microfluidic device to incorporate both AMs and VMs in ring-shaped EHTs [29]. First, AMs and VMs were differentiated and then embedded in a collagen-hydrogel to create chamber-specific, ring-shaped, EHTs. Zhao et al. developed a new Biowire platform for heteropolar tissues containing both atrial and ventricular ends for electrophysiology and drug responses (figure 1.3D) [63]. AMs and VMs were separately differentiated and then formed to myocardial tissues consisting of multiple cell sources in a hydrogel.

Those models are used for electrical stimulation of the heart tissue in order to promote cardiac maturation, but allows efficient screening of drugs with chamber-specific responses. Still, those models require multiple manual handling steps since cells are dissociated, sorted and re-seeded which is not advantageous. Asymmetric differentiation directly on chip is better since stem cells and CMs are very sensitive to slight changes in the differentiation protocol [70].

## 1.5 Thesis aim

As described, the protocol of Schwach et al. describes hPSCs-derived AMs and VMs but is limited in combining these different subtypes. Some OoC systems can provide 3D culture or maintain multiple cell sources but are limited asymmetric differentiation. Therefore, **the main goal of this research is to set up requirements for a microfluidic chip design that enables trapping EBs and subsequent asymmetric differentiation towards AMs and VMs**. For fabricating a microfluidic chip, requirements have to be defined:

1. Standard hPSCs differentiation towards AMs and VMs will be performed to replicate the RAR$\alpha$ protocol. This is important to rule out systematic errors and to ensure quality control.

2. Geometries of the chip design depend on the EB size these should be investigated in regard to the chip dimensions. Multiple seeding densities will be tested to determine and study the effect on EB size and differentiation.

3. For asymmetric differentiation, a steep gradient of this RAR$\alpha$ selective agonist should be obtained. Thus, the transition in AM and VM induction should be defined using various BMS-753 concentrations for combining the atrial and ventricular phenotype in one EB.

4. Various chip designs should be designed, fabricated and tested for trapping and differentiating EBs towards AMs and VMs to identify new requirements. Previous subgoals should be integrated in those designs.

# 2 | Materials and methods

This chapter explains the materials and methods that were used. Cell culture experiments were carried out at the Applied Stem Cell Technologies (AST) group in the ML-1, ML-2 and BioImaging Centre (BIC) and chip fabrication was carried out at the BIOS Lab-on-a-Chip group, and microfab lab at AST all at the University of Twente in the Netherlands.

## 2.1 EB-based differentiation of AMs and VMs from hPSCs

Differentiation was adapted from a previously described RAR$\alpha$-mediated protocol (figure 2.1) [33], but is briefly described. This protocol induces the atrial or ventricular phenotype by manipulation of the RA signaling pathway using BMS-753. By using the COUP-TFII$^{mCherry}$-NKX2.5$^{eGFP}$ hPSC line, AMs and VMs can be identified due to insertion of the red fluorescent mCherry sequences into the DNA (deoxyribonucleic acid) of chicken ovalbumin upstream promoter transcription factor II (COUP-TFII), which is an atrial specific transcription factor, within the well-established NKX2.5$^{eGFP}$ hPSC line [31]. These hPSCs are grown in Essential 8 (E8) medium (Gibco) and can be differentiated toward AMs and VMs via EB differentiation by resuspending them in the EB formation medium and aggregating them to EBs one day before the induction of cardiac mesoderm.

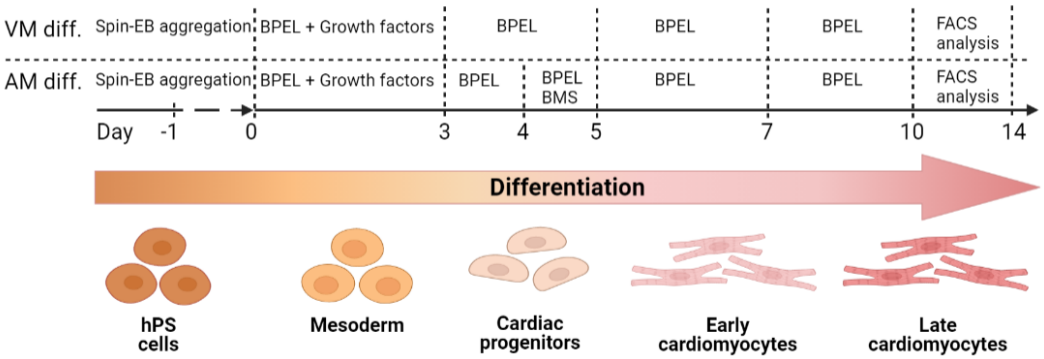


FIGURE 2.1: Schematic step-by-step representation of ventricular differentiation towards VMs and RAR$\alpha$-mediated atrial differentiation toward AMs by adding RAR$\alpha$ selective agonist BMS-753 on day 4. VMs show expression of RFP after day 4 and AMs show expression of both RFP and GFP after day 7.

### Formation of EBs from hPSCs

HPSCs were cultured in a monolayer on a vitonectin coated 6 wells cell culture plate (Cellstar). To fill one 96 wells plate (Greiner Bio-One) with EBs, one well of the 6 wells plate was used. Beforehand, E8 medium was already warmed to room temperature until it is no longer cool to the touch. The medium cannot be warmed to 37°C or in a water bath, because this can influence the supplements in the medium. At first, hPSCs were washed with DPBS

(Gibco). EDTA (0.5 mM, Invitrogen) was added for around 3 minutes and carefully removed (without removing the cells) afterwards. By adding 1 mL of E8 medium followed by gently pipetting up-and-down with a P1000, the cells were collected. After staining and counting with Trypan Blue, the hPSCs were resuspended in the required volume of E8 medium to achieve the necessary density ranging from 1k to 5k. Additionally, the necessary components poly (vinyl alcohol) (PVA, 400 $\mu$g/mL stock, Sigma Aldrich) in ratio 1:50 and ROCK Inhibitor (Y-27632, 10 $\mu$M stock, Bio-Connect) in ratio 1:1000 were respectively added to the E8 medium of the cell suspension. hPSCs were carefully seeded at the necessary density (mostly 5k was used) per well in a v-shaped 96 wells plate. In each 96 well plate, 60 wells can be used for making EBs. The outer ring of wells was filled with 150 µl DPBS to keep the humidity good for 14 days. For experiments with various densities (1k to 5k), at least 5 replicas were formed. hPSCs will aggregate by gravity and form the EB. On day 0 the cardiac mesoderm phase was induced by using several growth factors.

### Cardiac mesoderm induction

In the first step, the cardiac mesoderm phase is induced. First, the newly formed hPSCs EBs were washed with BPEL (bovine serum albumin (BSA) polyvinylalchohol essential lipids) medium (composition is described in [33]) to get rid of the E8 medium. Cardiac mesoderm was induced in the presence of a cocktail of growth factors composed of activin-A (Act-A, Miltenyi Biotec), bone morphogenetic protein 4 (BMP4, Miltenyi Biotec), the small molecule inhibitor of glycogen synthase kinase-3ß (CHIR-99021, Tocris Bioscience), vascular endothelial growth factor (VEGF, Miltenyi Biotec), and stem cell factor (SCF, Stem Cell Technologies) in BPEL medium for the initial 3 days of differentiation. In table 2.1 an overview of the amounts of growth factors needed for one 96-wellsplate is shown. For 60 wells in such a plate, these growth factors were added to 3.5 mL of BPEL. Important to notice is that BMP4, VEGF, SCF, ACT-A need to be cold, and CHIR needs to be protected from light at room temperature. Add 50 $\mu$L were added per well of total volume, including growth factors in BPEL. On day 3, the EBs were refreshed with BPEL to get rid of the growth factor solution. The next day (day 4), the induction of the atrial and ventricular phenotype was started.

TABLE 2.1: Overview of the amounts of growth factors needed for induction of cardiac mesoderm on day 3 [33].

| Growth factor | Storage (°C) | Stock (ng/$\mu$L) | Needed (ng/mL) | Volume to add ($\mu$L) for 1 plate |
|---|---|---|---|---|
| BMP4 | -80 | 25,00 | 20,00 | 2,80 |
| VGEF | -80 | 50,00 | 30,00 | 2,10 |
| SCF | -80 | 40,00 | 30,00 | 3,50 |
| Activin-A | -80 | 25,00 | 40,00 | 4,20 |
| CHIR ($\mu$M) | -30 | 4,00 | 1,50 | 1,31 |

### Induction of the atrial or ventricular Phenotype

On day 4, the EBs were refreshed with the RAR$\alpha$ selective agonist BMS-753 (10 mM stock, Tocris Bioscience) to induce the atrial phenotype. Concentrations ranging from 0.02 till 20 $\mu$M BMS were used for quantifying the switch between the atrial and ventricular phenotype. Important to notice is that BMS is sensitive to light, temperature and air, hence quick handling in the dark on ice is needed. The EBs were exposed to BMS for 24 hours, after which medium was refreshed with plain BPEL medium (day 5). For the generation of VMs, the EBs were kept in plain BPEL medium (100 $\mu$L/well) from day 3 until day 7.

## 2.2 Analysis during differentiation

During and after formation of AMs and VMs from hPSCs, multiple characterizations and analysis were performed on the cells.

### EB growth

The EB diameter over time was measured by taking pictures with an EVOS microscope once a day and the diameter was measured by hand using ImageJ. Different seeding densities of hPSCs varying from 1k to 5k were used for the formation of EBs and were analysed. The diameter of at least five EBs were measured for each seeding density.

### Fluorescent imaging

Differentiation into AMs and VMs was confirmed by fluorescence imaging of the COUP-TFII$^{mCherry}$-NKX2.5$^{eGFP}$ reporter line [31]. VMs show expression of NKX2.5$^{eGFP}$ after day 4 and AMs show expression of both COUP-TFII$^{mCherry}$ and NKX2.5$^{eGFP}$ after day 7. From day 7 until day 14 fluorescent images were taken using the Nikon ECLIPSE Ti2 (Nikon Instruments Inc. USA). Fluorescence images were analysed using ImageJ (Java).

## 2.3 Characterization of AMs and VMs

### Dissociation of EBs for further characterization

To further analyse the EBs, dissociation was performed at day 14 to obtain single cells. Per condition 5 or 10 EBs were combined in one sample. The BPEL medium was aspirated from the cells and then washed with DPBS. Depending on the amount of EBs, either 50 $\mu$L BPEL and 5 $\mu$L collagenase (Worthington, Biochemical) for 5 EBs or 100 $\mu$L BPEL and 10 $\mu$L collagenase for 10 EBs was added to the samples and incubated for 20 minutes at 37°C. Next, the collagenase and BPEL were removed and the samples were washed with 1 mL DPBS. Per sample 500 $\mu$L (EBs should be covered) of 10x TriplE (Gibco) was added and incubated for 5-10 minutes at 37°C. Cells were carefully dissociated by pipetting up and down with a p1000 Biosphere pipette tip. CMs are sensitive to mechanical dissociation, so it is recommended not to pipette too harshly. Three times more PEB buffer (protein extraction buffer, Gibco) (1500 $\mu$L) as TriplE was added to the samples to dilute TriplE. Next, samples were spun down at 240 g for 3 minutes. After removing supernatant, the pellet was resuspended in 400 $\mu$L PEB buffer and transferred to Flowtubes (Falcon) (used for flow cytometry or FACS). The dissociated samples were placed on ice and immediately analyzed for determining the percentage of the GFP and mCherry fluorescence with a flow cytometer by FACS.

### Flow Cytometry Analysis or FACS

Single cell analyzis was performed with a flow cytometer (MACSQuant VYB from Miltenyi Biotec) to quantify the percentage of AMs and VMs at day 14 or day 15. Each cell is analysed for visible light scatter and one or multiple fluorescence parameters. The principle of a fluorescence-activated cell sorter (FACS) is shown in figure 2.2a. Cells were counted and multiple parameters were measured simultaneously. In this case, the size of the cells and the proteins expressed by the cells were determined . AMs are selected by NKX-2.5-GFP+ and COUP-TFII-mCherry+ (for RFP) expression and as a control VMs are selected by NKX-2.5-GFP+ and COUP-TFII-mCherry- expression. The system was calibrated using microbeads according to the manufacturer protocol. Samples were kept on ice and loaded inside the Chill5 rack (MACS Miltenyi Biotec). The Cardiomyocytes-mCherry program was selected and Gate 3 was set to count 10000 cells instead of the whole sample to process them faster.

The loaded sample was excited using both a 488 nm laser for GFP fluorescence and 561 nm for mCherry fluorescence and recorded for 10 seconds.

Subsequent data analysis was performed with FlowLogic software (FlowJo software) analysis, and the results were expressed as the percentage of positive or negative cells. First, a distinction between single cells and clumps is made its forward scatter intensity value (cell size), and its side scatter intensity value (cell granularity). Next, the difference in NKX2.5$^{eGFP}$ and COUP-TFII$^{mCherry}$ is determined in the final scatter plot. Each data point represents an individual cell. Both axis represents the intensity of either the GFP or mCherry fluorophore. A schematic example of the final output is shown in figure 2.2b. Percentages of AMs and VMs after different treatments were gathered.

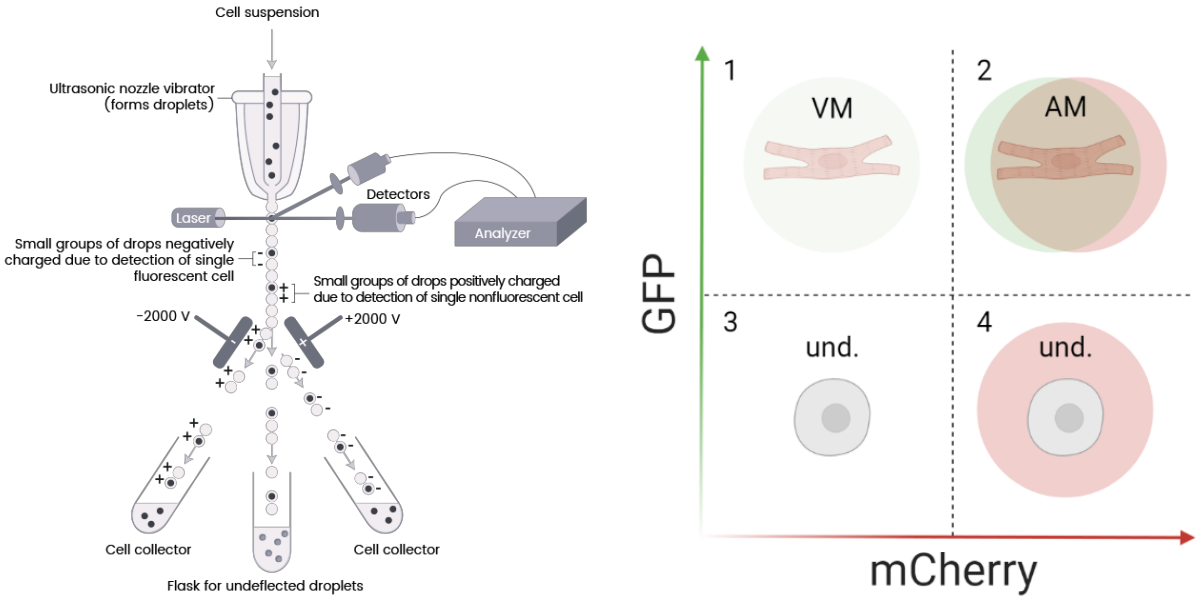


(A) Method (B) Output

FIGURE 2.2: (A) The principle of FACS. (B) Schematic example of the four quadrants of a FACS scatter plot. The X-axis is the intensity of red fluorescence. The Y-axis is the intensity of green fluorescence. Quadrant 1 shows many green fluorochromes but no red ones which represents the VMs. Data points for AMs with high levels of both green and red fluorochromes will appear in quadrant 2. If cells have neither green nor red fluorochromes, the data will appear in quadrant 3. Data for cells with many red fluorochromes and no green fluorochromes attached will appear in quadrant 4. Quadrant 3 and 4 are undefined (und.) cells. Images adapted from Biorender.

## 2.4 Design of chips

A 3D model of the chip has been designed with the computer aided design (CAD) software SolidWorks (Dassault Systems, France). This model was translated into G-code, a numerical control programming language, for milling via the computer aided milling (CAM) with the Autodesk HSM software (SolidCAM, USA). Technical drawings from the CAM models can be found in Chapter 3.

## 2.5 Fabrication of chips

Chips were milled out of a 8.0 mm thick polymethyl methacrylate (PMMA) substrate using a CNC mill (Datron AG, Germany) with HSC pro software (Datron AG, Germany). Double fluted end mills with a flute diameter of 5.0 mm, 1.0 mm and 0.5 mm were obtained from

Datron (Mühltal, Germany) and used to mill into the PMMA. After milling of the PMMA, chips were fabricated using PDMS (Permacol RTV615) in a 1:10 weight ratio of base vs. curing agent. The stirred and degassed PDMS was poured on the PMMA mould, degassed again, and cured at 65°C for 3 hours up to overnight. Cured PDMS was removed from the mould and cut to size. Inlets and outlets were punched using a 1 mm biopsy puncher with pluncher (Ted Pella, Miltex). Glass slides (Corning, 75x50 mm, 1 mm thick) and PDMS chips were assembled on top of each other after activation by oxygen plasma using a plasma cleaner (CUTE, Femto Science, Germany). Chips were placed in storage covered with adhesive tape, until further use.

### 2.5.1 Flow and control layer fabrication

Chip design 3 consists of a flow and control layer which were milled with a mill diameter of 1.0 mm.For the flow layer, a stirred and degassed PDMS mixture (1:7 w/w, curing agent to base polymer) was poured on top of the PMMA mold. The control layer was fabricated by spin coating a PDMS mixture (1:20 w/w, curing agent to base polymer) on top of the mold using a spin coater (SPS SPIN 150). The mold with 0.5 mm channels was spin coated at 300 rpm for 20 seconds, while the mold with 1 mm channels was spin coated at 150 rpm for 10 seconds. Glass slides were also spin coated (300 rpm for 30 seconds) with PDMS (1:20 w/w, curing agent to base polymer) for better adhesion of the layers since the milling roughness is transferred to the PDMS layers.

Afterwards, all molds and glass slides were cured in an oven for 45 minutes at 65°C. When the PDMS was partially cured, the flow layers were removed from the mold. First, 1 mm holes were punched to create flow inlets and outlets. Next, one of the flow layers was aligned on top of the control layer and control inlets were punched with the same 1 mm hole puncher. Both layers were then assembled on the PDMS-coated glass slide without plasma treatment. The top of the chip was covered with adhesive tape and another glass slide was pressed on top using two clamps to evenly divide the pressure. To fully cure, the whole chip was placed overnight in the 65°C oven. For food coloring characterization or cell culture, the whole chip was plasma treated to clean the chip and to make it hydrophilic.

## 2.6 Differentiation of AMs and VMs from hPSCs on chip

First, EBs were formed in a standard V-shaped 96-wells plate on day -1. On day 0, EBs were seeded on the chip and cardiac mesoderm induction was performed by adding growth factors as described in section 2.1. On day 4, the atrial phenotype or ventricular phenotype was induced by either adding no or 20 $\mu$M BMS. Since the volume on chip is smaller, hence pipette tips were used as extension the same steps were followed as the standard differentiation protocol.

## 2.7 Characterization of AMs and VMs on chip

Analysis during culture was performed by measuring the EB size and fluorescence imaging of the COUP-TFII$^{mCherry}$-NKX2.5$^{eGFP}$ reporter line. From day 0 till day 14, EBs were measured using the EVOS. Fluorescence images were made from day 4 until day 14 using the Nikon ECLIPSE Ti2.

# 3 | Results and discussion

This chapter presents and describes the obtained results towards the aims stated in the thesis aim in chapter 1.

## 3.1 Replication of the RAR$\alpha$ protocol in the ML-1 student LAF cabinet versus the BIC LAF cabinet

Stem cells and cardiomyocytes are very sensitive to DNA damage and undergo rapid apoptosis even after low-damage doses or slight changes in the differentiation protocol [70–72]. Especially, day 0 until day 3 (mesoderm induction phase) are essential for a successful differentiation further on [33]. On day 0, growth factors are added to go from hPSCs to the cardiac progenitor stage. It is essential that the amount of growth factors is really precise. Multiple parameters have changed in the protocol compared to the original protocol. Another researcher (the author of this thesis) that had no experience specifically in stem cell differentiation performed the protocol in another lab (ML-1) and used different equipment. To replicate the standard protocol differentiation yields were compared and morphological observations were performed. The expected differentiation efficiency using this protocol is around 70% AMs + 5% VMs out of the total cell population. Considering only the cardiomyocyte population, 94% AMs + 6% VMs are differentiated from the RAR$\alpha$ protocol. Those percentages were found when using 20 $\mu$M selective agonist BMS-753 while the protocol was performed in the BIC laboratory. However, it soon appeared that the differentiation efficiency was low compared to Schwach et al. [33]. Only around 20% total amount of cardiomyocytes were produced (see left graph in figure 3.1).

To rule out systematic errors made by the inexperienced stem cell researcher, the results were checked by an experienced stem cell researcher. The use of growth factors solutions prepared in the BIC by the experienced researcher was first changed. In figure 3.1 the first graph shows the original results in the ML-1 student LAF cabinet. The second graph shows the results with the use of prepared growth factor solutions. For low BMS concentrations the total CM population was around 70%, but still the percentage for 20 $\mu$M BMS was low (around 10%).

A parameter that was noticed to be crucial is the laboratory equipment, especially the pipettes (Pipetman) since the cultures in the BIC have a higher success-rate. It could be that those in the ML-1 student LAF cabinet are not properly calibrated which has a big influence on small volumes. Moreover, it was observed that the incubators also play an important role in the differentiation efficiency. First, pipetting was done more carefully in the ML-1, but did not make a difference.

Another variable that had influence on the effectiveness of differentiation was the incubator. Those in the ML-1 were used extensively by many students. Most of them work with cells that are much less sensitive, thus do not encounter the effect of opening and closing the incubator on this protocol. As a consequence, it was decided to do the full differentiation

protocol in the BIC ML-2 which resulted in the best results that were obtained in this thesis (right graph in figure 3.1). Out of the total cell population, around 10% AM + 70% VM were differentiated using 0, 0.5, or 1 $\mu$M BMS, while approximately 35% AM + 3% VM were differentiated using 20 $\mu$M BMS. Further differentiations were performed in the BIC ML-2, since those laboratory equipment came out as most successful differentiation.

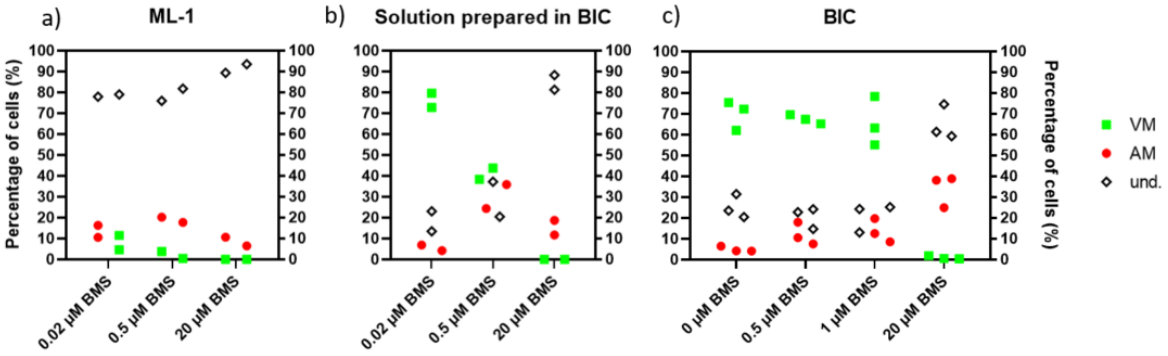


FIGURE 3.1: Scatter plot graphs representing the flow cytometry results of the a) student LAF cabinet ML-1 (n=2), b) preparation of solutions in BIC (n=2), and c) BIC ML-2 (n=3).

Finally, it was demonstrated that the CM yields using the RAR$\alpha$ protocol with lower BMS concentrations ($\sim$15% AMs + $\sim$50% VMs for 1 $\mu$M BMS) are as high as or nearly as high as original ($\sim$30% AMs + $\sim$55% VMs for 1 $\mu$M BMS) when working in the BIC. On the other hand, when using 20 $\mu$M BMS in the original protocol gives 70% AMs + 5% VMs but in this project only 35% AM + 3% VM were differentiated. Differences may be due to the enrichment of AMs. Based on metabolic selection and monolayer plating that was included into the protocol of Schwach et al. [33]. This was to obtain highly purified CM populations (>90% CMs) [73]. The beating AMs at day 13 were dissociated and plated on vitronectin-coated well plates [33]. They observed that this purification was less efficient in EB format because of limited diffusion of the medium to the inner corner of the EBs. Furthermore, they discovered that maintaining EBs more than 21 days and exposed to cardiomyocyte medium, their dissociation became more difficult, resulting in higher cell loss. To ensure that all cells had equal access to the medium and that the recovery of CMs was simple and stress-free for the cells, they included an intermediary step of monolayer plating was included. However, this was not included in currently used protocol since for this study the focus was to form both VMs and AMs in an 3D format. For this reason, this extra step of monolayer plating is not useful in a microfluidic chip.

## 3.2 EB growth over time using different initial cell seeding densities

One of the parameters for setting up requirements for the chip design is to characterise the EB size over time. The size is important to know for dimensions in the chip design. Smaller EBs could lead to smaller channels, less growth factors, and more parallelizable conditions.

To determine the size of an EB throughout the whole differentiation protocol, EB diameters were measured from day 0 till day 14. Different seeding densities of hPSCs varying from 1k to 5k were used for the formation of EBs and were analysed because 5k cell seeding density is standard used. The protocol was kept the same for all densities. It was observed that 1k and 2k seeding densities were too low for forming compact round looking EBs, and

4k seeding density did not differ much from 5k seeding density. Experiments were continued with 3k and 5k seeding density. In total, 6 EBs from each condition were measured over a full-term culture of 14 days. From day 7 and on, the EBs started beating. Images were made in relaxed state, but it should be kept in mind that from this day on the results.

Images of two EBs are shown over a period of 14 days, one with 3k seeding density and one with 5k seeding density in figure 3.2a. It is observed that the EBs do not have the same shape every time point, but are still round. This observation may be due to the fact that the EBs are able to move freely through the well. This also made it not possible to measure in the same angle every time point.

In figure 3.2b a graph of the diameter of the 3k and 5k EBs over the 14 days are shown. It is observed that there is no big difference overall between a seeding density of 3k and 5k cells From day 0 till day 5, the EBs grow and after that they start to compact. This means that the peak in diameter is obtained at day 5. In the end the EBs have a diameter of around 1 mm. At day 7 a bigger difference in diameter is found between 3k and 5k cell density.

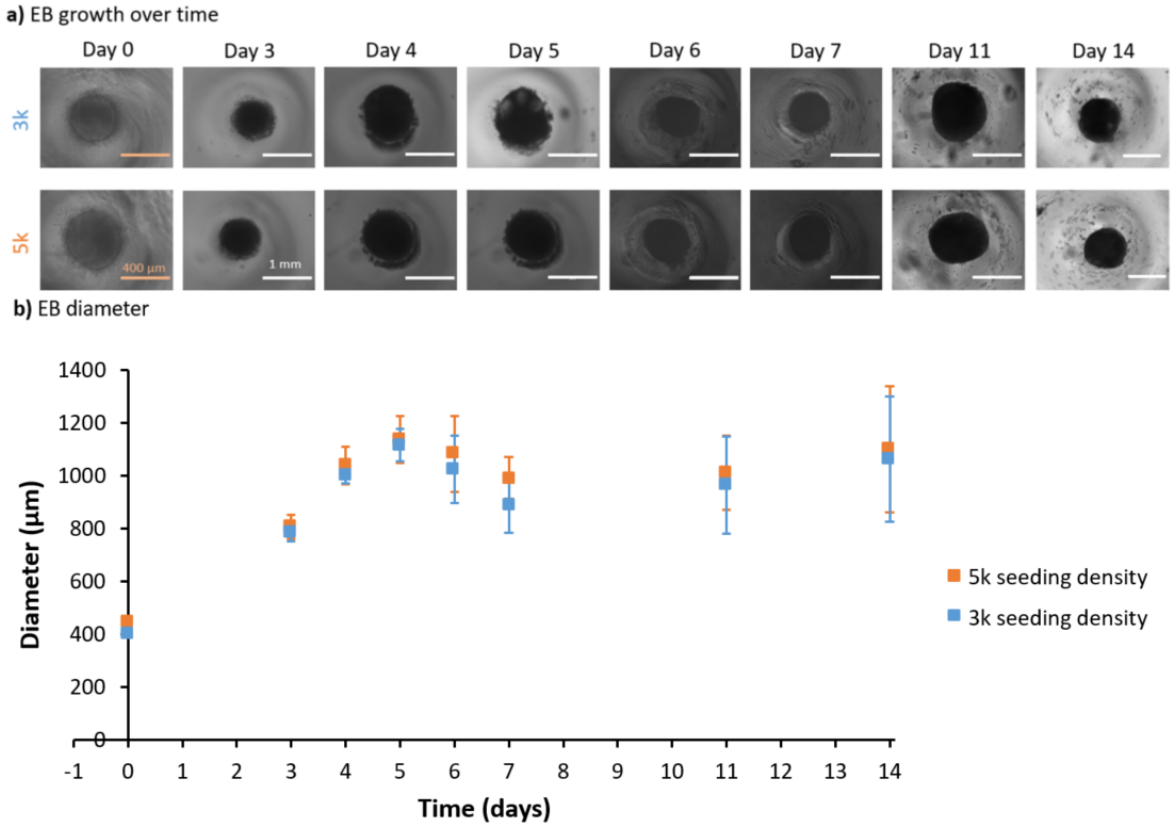


FIGURE 3.2: Growth over time followed for 14 days. After this, the EBs started contracting and the size measurements are not accurate anymore. a) A 3k and 5k EB are shown over time. b) The measured growth over time in days is shown (n=6). Scale bars: 400 $\mu$m (day 0) and 1 mm (day 3-14).

Larger standard deviation on days 11 and 14 is observed indicating that there is a lot of variance in the observed data around the mean. Possible reasons may be the compaction and the beating of the EBs. Every EB beat differently causing variety in shape and thus could affect the diameter.

In the end, those results mean that the microfluidic chip should at least have a diameter of 1 mm. Channels could be around 500 $\mu$m because the EBs are still around 400 $\mu$m at day 0. This is not possible when the EBs have to be removed after 14 days of culture to perform

flow cytometry analysis. One thing to keep in mind is that on chip the volume is (mostly) smaller than in a wells plate.The volume of medium used in a wells plate is between 50 and 150 $\mu$L, while most microfluidic channels have volumes in the range of nL or $\mu$L [60]. This can influence the behaviour of the micro-environment.

## 3.3 Transition in AM and VM induction using different BMS concentrations

For combining the atrial and ventricular phenotype, it is important to define the transition in AM and VM induction by using different BMS concentrations. To achieve this, concentrations ranging from 0.02 to 20 $\mu$M BMS were tested. In addition, all BMS concentrations were tested both on EBs formed out of 3k seeding density and 5k seeding density.

The fluorescent images in figure 3.3a show the results of the lowest (0.02 $\mu$M BMS), middle (2 $\mu$M BMS) and highest (20 $\mu$M BMS) are shown. NKX2.5$^{eGFP}$ is a fluorophore for CMs in general, while COUP-TFII$^{mCherry}$ fluorescence is specifically for AMs. As can be seen, the lowest BMS concentration resulted in the most NKX2.5$^{eGFP}$ expression and lowest COUP-TFII$^{mCherry}$ expression meaning that mostly VMs are differentiated. On the other hand, the highest BMS concentration resulted in the same NKX2.5$^{eGFP}$ expression but highest COUP-TFII$^{mCherry}$ expression meaning that this BMS concentration resulted in mostly AMs. The BMS concentrations of 2 and 20 $\mu$M resulted in both NKX2.5$^{eGFP}$ and COUP-TFII$^{mCherry}$ expression, which represents a mixed population of VMs as well as AMs. Those results are similar when comparing to the results of Schwach et al. who tested 1, 10, 15 and 20 $\mu$M BMS [33]. Moreover, in the fluorescent images can be seen that the AMs and VMs are mixed and not divided into two even parts. This is a result of having no gradient of BMS.

Flow cytometry was performed to get more insight in the actual cell population by determining the percentages of AMs and VMs that were differentiated. The sample size ($n$) is very small (between n=1 and n=5), so only the individual data points are plotted [74]. The results in figure 3.3 obtained with 5k seeding density showed higher percentages of cardiomyocytes out of the total cell population. Looking at both 3k and 5k results in the graphs of the combined FACS results (figure 3.3b), treatment with 0.02 and 0.1 $\mu$M of BMS resulted in mostly VMs.

On the other hand, only looking at the AM and VM population, treatment with 2 until 20 $\mu$M of BMS resulted in mostly VMs. Treatment with 12.5, $\mu$M BMS resulted in a higher percentage of AMs than 20 $\mu$M of BMS. Compared to Schwach et al., this was not expected. Nevertheless, the percentages are still relatively low compared to the results of Schwach et al. who obtained 70% AMs + 5% VMs out of the total cell population. Still the highest percentage of those treatments are undefined cell types. To further improve those results, more replicas should be obtained.

One of the requirements in this project is to find the transition in AM and VM induction. With those results it is shown that treatment with 0.5 and 1 $\mu$M of BMS resulted in a mixed population of AMs and VMs. Transition of differentiating AMs and VMs is shown around those treatments.

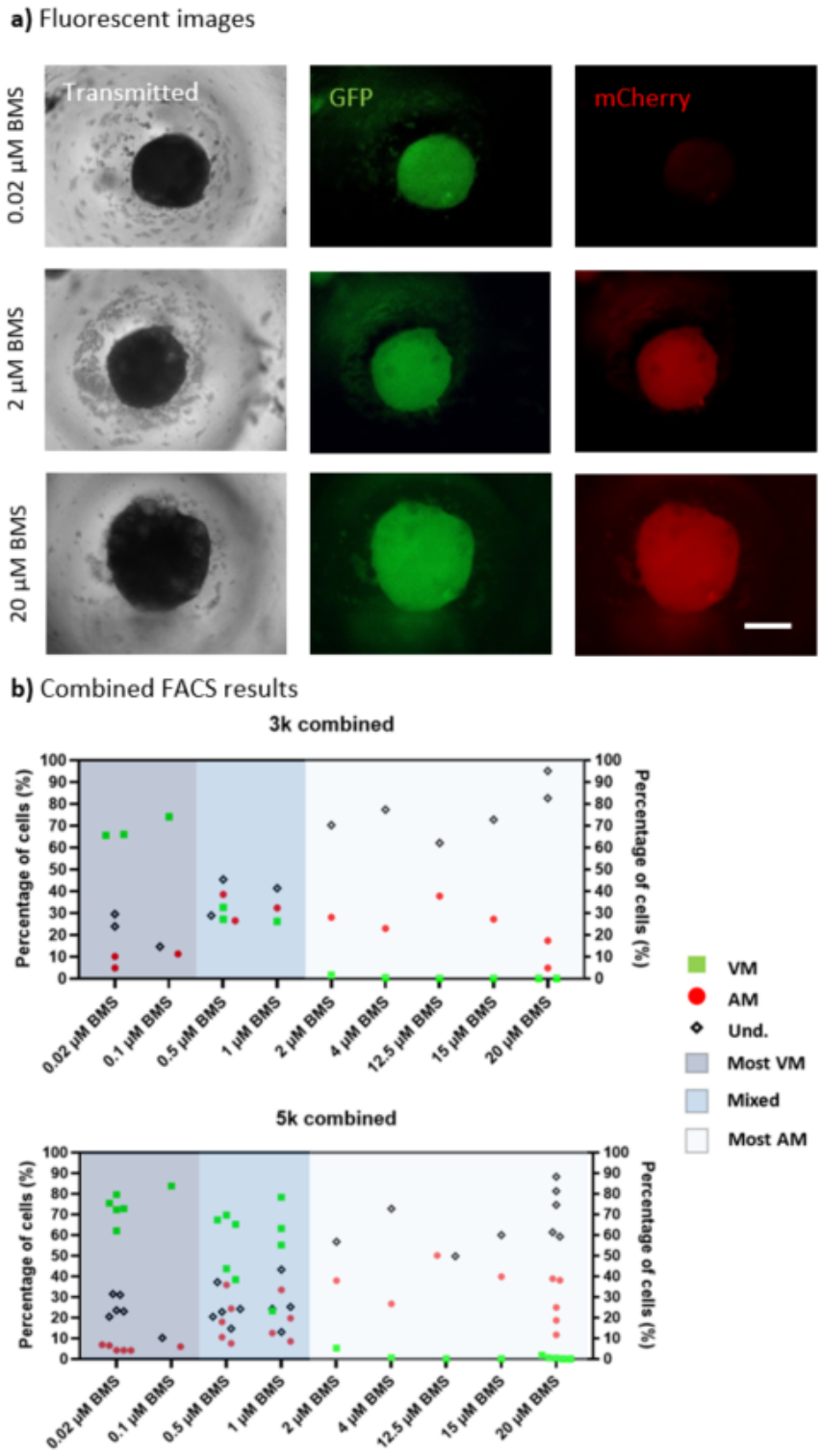


FIGURE 3.3: a) Transmitted and fluorescent images on day 14 of three EBs treated with 0.02, 2 and 20 $\mu$M BMS. b) Obtained results from different concentrations BMS on both 3k and 5k cell seeding densities in two scatterplots. The gradient is only focussed on the AM and VM population, not on the undefined cell types. All differentiations were conducted in BIC ML-2. Scale bar: 1000 $\mu$m. und. = undefined cell population.

It is noticed that for concentrations higher than 0.5 $\mu$M BMS for 3k and higher than 2 $\mu$M BMS for 5k the undefined cells are the highest. A possible reason for this could be that there were still small changes in the protocol of the inexperienced stem cell researcher. Results of treatment with 20 $\mu$M BMS using the same stem cell passage number in the same laboratory with the same cell seeding density were compared to those of the experienced researcher. The differentiation of the inexperienced researcher researcher resulted in $\sim$40% AMs+ $\sim$2% VMs while the differentiation of the experienced researcher resulted in $\sim$70% AMs+ $\sim$5% VMs (see appendix figure A.2).

When looking at the graphs separately it is noticed that the 5k cell seeding density resulted in higher percentages overall ($\sim$70% CMs for 5k, and $\sim$60% CMs for 3k). In the previous section was shown that using either 3k cell seeding density or 5k cell seeding density does not result in a significant difference in the size of the EBs. Nevertheless, the obtained AM and VM percentages are higher when using EBs formed with 5k cells compared to EBs formed with 3k cells. This is the standard and thus the protocol is optimized for that.

Initial cell seeding density as one of the culture conditions has been shown to have tremendous effect on cell proliferation, differentiation, and extracellular matrix (ECM) synthesis [75, 76]. Those studies showed that cell density is an important factor can promote cell proliferation and differentiation. Schwach et al.'s results suggest that the higher differentiation rate is possibly due to increased cell-cell interaction and cell density depends influence of growth factors [77]. Thereby, the generation of atrial cells depends on an appropriate mesoderm population, which means the first phase of differentiation is the most important phase [32]. To get such a appropiate mesoderm population, it is shown that AMs needs more cells for development than VMs [32]. Comparing this to our own results could explain why the atrial population using 3k cells is lower than when using 5k cells to form an EB. For this reason, only 5k is used in all remaining experiments.

To conclude, these results mean that the standard 5k cell seeding density results in higher percentages of both AMs and VMs. A mixed population is obtained with 0.5 and 1 $\mu$M BMS. For the microfluidic chip requirements it means that the steep gradient should obtain those concentrations. As a minimum requirement for BMS concentration on either side of the EB to obtain a predominantly AM side and a predominantly VM side, a concentration higher than 2 $\mu$M BMS should be used for the AM side and a concentration lower than 0.1 $\mu$M BMS should be used for the VM side. Thereby, it should be taken into account for diffusion through the EB that the EB diameter on the day of adding BMS (day 4 in the protocol) is already around 1 mm.

## 3.4 Chip design, characterization and proof-of-concept cell culture

This section presents and discusses three microfluidic chip designs that were developed. It is important to trap the EB in a defined location. Having the EB in an undefined location results in not knowing the effect of the gradient on the differentiation process. The chip molds were successfully fabricated using the Datron micro-mill and chips were fabricated with PDMS.

### 3.4.1 Pillar inspired microfluidic trapping system

One of the requirements of the chip design is to trap an EB. Creating 3D cell aggregates and prolonged culture with optimized conditions in microfluidic trapping systems was previously utilised by Khoury et al. [58]. A pillar-inspired design was developed from this.

Figure 3.4 shows the design with on the left three different looking designs, with all three inlets and three outlets. Here, it was chosen to have a variable chamber for testing the guidance of the EBs towards the trap. Originally, those outer two inlets and outlets should be used for creating a BMS gradient in the chamber by adding a high concentration at one side and a low concentration on the other side. However, at first the cells were trapped and the standard differentiation protocol was tested. Thus, the side inlets and outlets were not needed. On the right panel in the figure the designs with just one inlet and one outlet are shown which were used for the first proof-of-principle hPSCs differentiation on chip. Each chamber includes a U-shaped microtrap construction consisting of round pillars (designed to be 200 $\mu$m in diameter with 10 $\mu$m spacing). This design meets the requirements of being able to trap an embryoid body and towards delivering various conditions of growth factors.

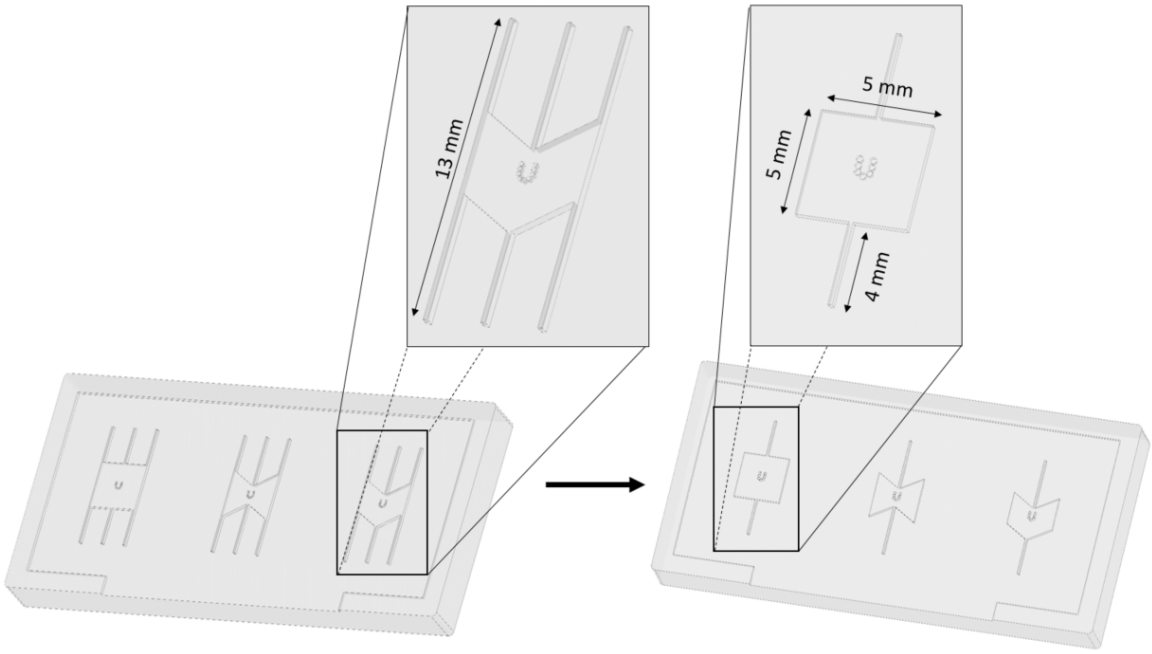


FIGURE 3.4: Pillar inspired microfluidic trapping system with either three inlets and three outlets on the left design and one inlet and one outlet at the right design.

#### 3.4.1.1 Characterization of micromilled pillars

Each chamber includes a U-shaped microtrap construction consisting of round pillars (200 $\mu$m pillar with 10 $\mu$m spacing). It was observed that those pillars were not separate, which could result in bad regulations in oxygen and nutrient levels as required for EB culturing and differentiation.

Characterization was carried out by milling a test platform that consists of various holes (negative mold). The hole diameters were 200, 300, or 500 $\mu$m and the space between the pillars 10, 50, 100, 200, 500 or 1000 $\mu$m (figure 3.5a). Holes of 200 $\mu$m were milled 1 mm deep, pillars of 300 $\mu$m were milled 200 $\mu$m deep, and pillars of 500 $\mu$m were milled 2 mm deep. After PDMS fabrication, pillars were obtained.

In figure 3.5b the systematic characterization of the separation of the pillars is shown. For this characterization images from the top view of the platform and images from the side view of the PDMS pillars were made and analysed. Pillars were indicated as separate when those are fully separate from top to bottom. Especially, the pillars with wider spacing are fully separate. Also it is noticed that all 300 $\mu$m pillars are fully separate.

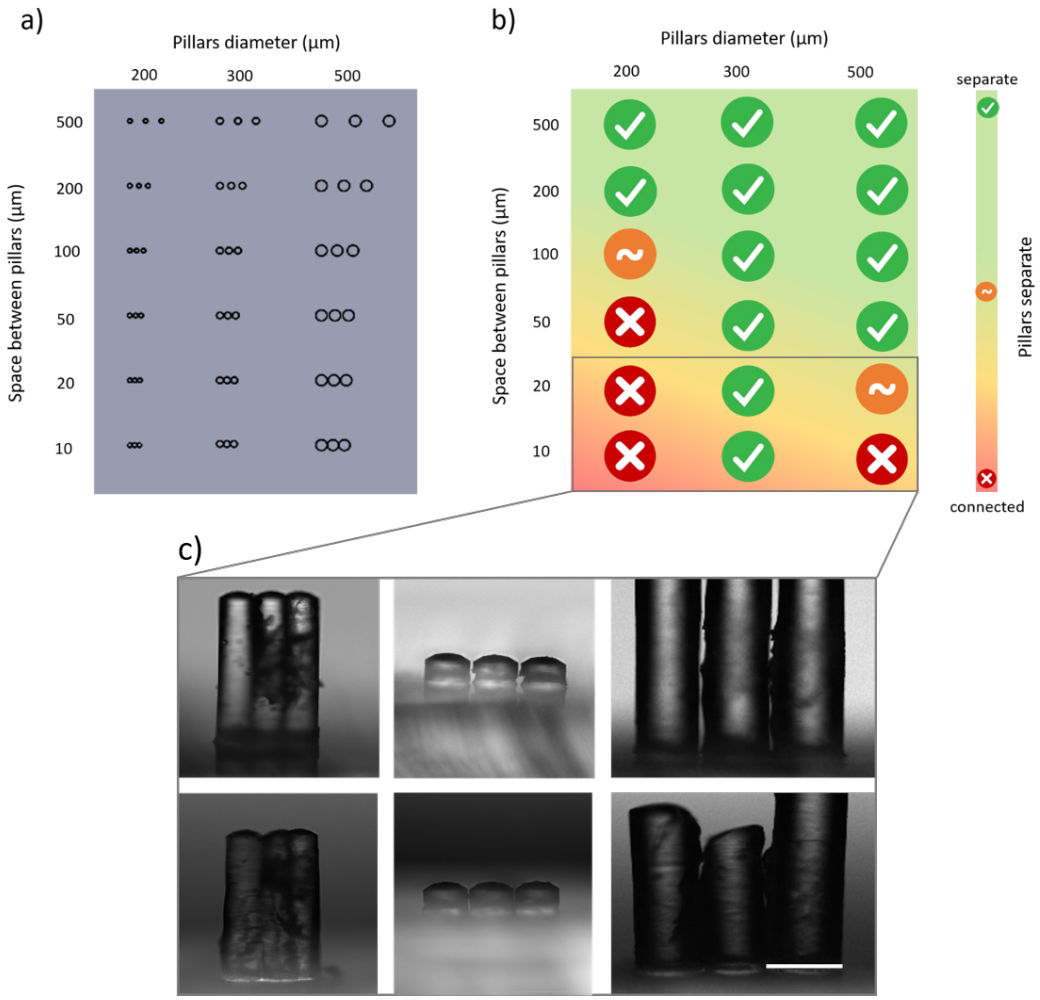


FIGURE 3.5: a) Characterization platform. b) Systematic characterization of separation of the pillars. Green check mark indicates full separation, orange approximate mark indicates half separation, and red cross indicates no separation at all. c) Close-up of PDMS pillars. Raw data can be found in Appendix A.3.

Narrowing the space between the pillars makes it more difficult to produce fully separated pillars. Some pillars are partially connected and thus those are marked with a approximate mark in the figure 3.5b. To further improve those results, more characterizations should be performed. Most of the pillars made with the 200 $\mu$m drill are not separate at all and fully connected. Those are marked with a red cross in figure 3.5b. This explains the observation of connected pillars within the chip design.

Results show that the 300 $\mu$m pillars with 10 $\mu$m spacing were separate, while the 200 $\mu$m pillars with 10 $\mu$m spacing were not. A reason for that could be that the 200 $\mu$m drill was used more often than the 300 drill and thus the 300 $\mu$m drill results in cleaner holes. If a new 200 um drill is used, better holes for this size may be obtained. It could also be due to the fact that the pillars of with 300 $\mu$m were shorter and thus less repeats of drilling were made. The more repeats, the more errors in misplacing the drill could occur and therefore result in less smooth pillars.

In conclusion, results of this characterization suggest that the pillars made with the 300 $\mu$m drill give the best results when looking at separation. Due to those results, the next design was made with the 300 $\mu$m drill.

#### 3.4.1.2 Cell culture in microfluidic trapping system

As proof-of-concept, EBs were seeded and cultured within the microfluidic trapping system. EBs were first formed inside a standard V-shaped 96-wells plate and used at day 0. The same protocol as a standard hPSCs differentiation towards the VM phenotype was followed (no treatment with BMS on day 4).

In total four EBs were seeded and trapped. However, two came out of the trap after a few hours. Nevertheless, two were successfully cultured for 14 days. After 10 days of culture it was observed that the EBs were beating and after 14 days of culture it was observed that NKX2.5$^{eGFP}$ was expressed (Figure 3.6). However, not the whole EB expressed NKX2.5$^{eGFP}$, only at the front part of the trap. This indicates that a gradient was formed [50]. Furthermore, the shape of the EB is different than that of one in a standard culture. Those observations indicate that the trap is too small for the EB, so it deforms, and thereby the trap is working as a wall for nutrients and prevent growth factors from fully diffusing through the EB.

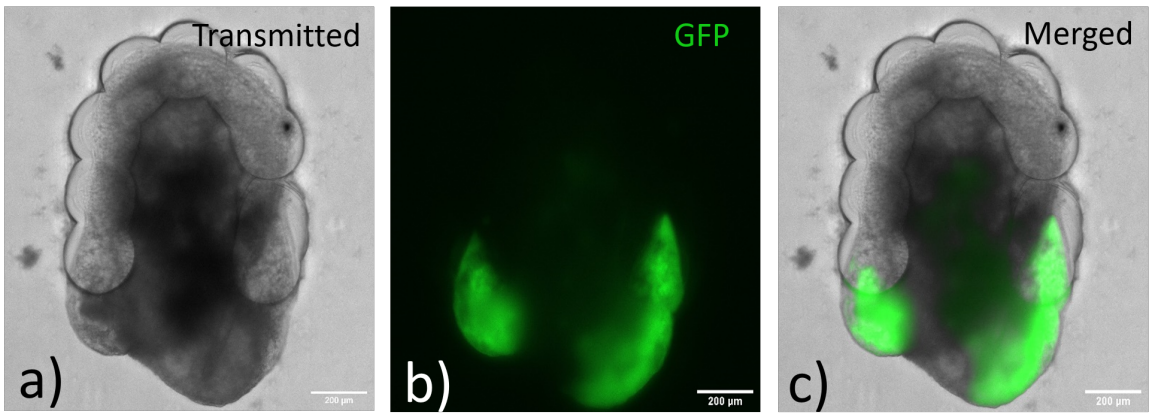


FIGURE 3.6: EBs cultured in microfluidic trapping system. a) Live-cell bright-field, b) fluorescence and c) overlay images of NKX2.5$^{eGFP}$ expressing (green). Scale bar: 200 $\mu$m. Images were made day 14 of culture.

Lastly, it was noticed that the chamber design does not influence the trapping mechanism. Fluid flow was not tested, but it is expected that the swallow tailed shape has a fluid flow profile guiding towards the trap while the other two shapes do not.

Finally, the chip meets the requirements of trapping an embryoid body and allowing differentiation to VMs. Two EBs were partially differentiated towards the ventricular phenotype. However, the next design should have a bigger trapping system.

### 3.4.2 Channel with pillar trap

Since the previous chip design was proven to be too small for the EB and the chamber did not add any value for the trapping process, a new design was utilised (figure 3.7). This design has just one straight channel of 1 mm (w) x 1 mm (h) x 10 mm (l) including a trapping mechanism that consist of either two or three pillars of 300 $\mu$m. The negative mold exists of 2 replicas of each channel.

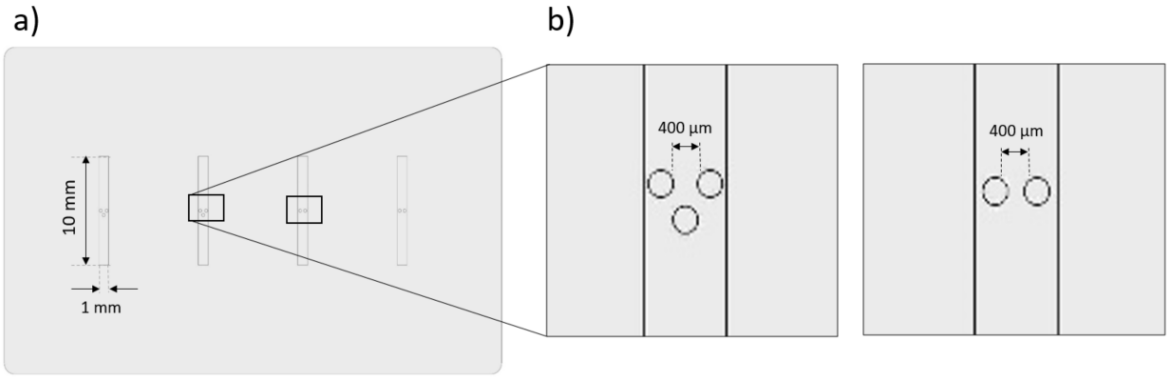


FIGURE 3.7: Channels with pillar trap. a) PMMA mold with four channels, b) close-up of trap.

#### 3.4.2.1 Cell culture in chip based on EB size

The same protocol was used to seed and culture EBs within the new design as a proof-of-concept cell culture. EBs were formed with 5k cell seeding density in a standard V-shaped 96-wells plate. Around eight EBs from day 0 were tried to seed in this chip. Only three were cultured for 14 days.

During the seeding at day 0 it was observed that the EBs were blocked by the pillars but could also move easily back to the channel inlet due to medium back flow. As a solution the chip was placed in a slope (5 mm) (figure 3.9) This ensured that the EB was forced inside the trap due to gravity. However, this resulted in more medium in the pipette tips at the outlets due to difference in hydraulic pressure.

Whenever the medium had to be refreshed or optical images were obtained the chip was placed flat instead of in the slope. Medium flow was caused by the difference in medium height inside the pipette tips and the EB moved towards the inlet or even inside the pipette tip. To keep the EB inside the trap, medium was refreshed by first removing medium in the outlet pipette tip and new medium was added to the inlet (without removing or replacing the pipette tips). This resulted in medium flow from the inlet to the outlet, because there was more medium at the inlet than at the outlet. Afterwards the chip was placed in the slope (back in its box), to ensure that the EB would stay in the trap overnight.

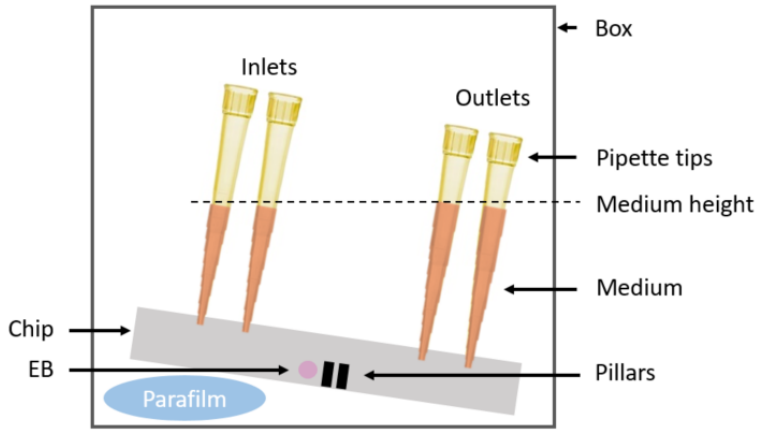


FIGURE 3.8: Schematic overview of refreshing medium.

The medium back flow when setting the chip on a flat surface again is calculated using the following formulas for the flow rate, hydraulic resistance in a square channel, and the difference in pressure:

$$Q = \frac{\triangle P}{R_H} \tag{3.1}$$

$$R_H = 28.4 \mu L \frac{1}{w^4} \tag{3.2}$$

$$\triangle P = \triangle h \rho g \tag{3.3}$$

where $Q$ is the flow rate, $\triangle P$ is the difference in pressure, $R_H$ the hydraulic resistance, $\mu$ is the dynamic viscosity of the fluid, $L$ the length of the channel, $w$ is the width of the channel, $h$ is the height of the channel, $\triangle h$ is the difference in fluid height, $\rho$ is the density of the fluid, and $g$ is the gravitational field strength. When it is assumed that there was a difference of fluid height in the pipette tips of 5 mm and only taking into account the hydryaulic resistance and volume of the chip channel, a back flow rate of $\sim 200$ $\mu$L/s was calculated. According to observations, this is an assumption of the back flow rate in the channel without including the pipette tips in the calculation. When the medium begins to flow, the EB is not moving yet. At some point the EBs starts moving but at the end the medium difference is less, so the flow rate and EB also slows down. It can be concluded that this design is very sensitive to even small height different in medium.

Moreover, the shape of the EBs shows an unusual morphology with bubble-like vesicles (see figure 3.9). This could be due to the problems during medium refreshment. The fluid flow during medium refreshment creates a lot of stress on the cells. Stem cells and cardiomyocytes are very sensitive and even after mild slight changes to the differentiation technique, stem cells and cardiomyocytes quickly undergo apoptosis [70–72].

Another reason of this unusual and unhealthy shape of the EB the shape of the trap. In a standard culture, V-shaped wells are used to enhance the round shape of an EB. Some EBs were cultured in the wells plate as control and those looked round as normally. The shape of those new pillars may therefore induce a different shape. Compared to the pillars of the previous trapping design, the EBs in this new design look worse. The trap in the previous design might be too small to enhance a full round shape, but since the EB is at a fixed place the rest of the EB looks like a normal EB.

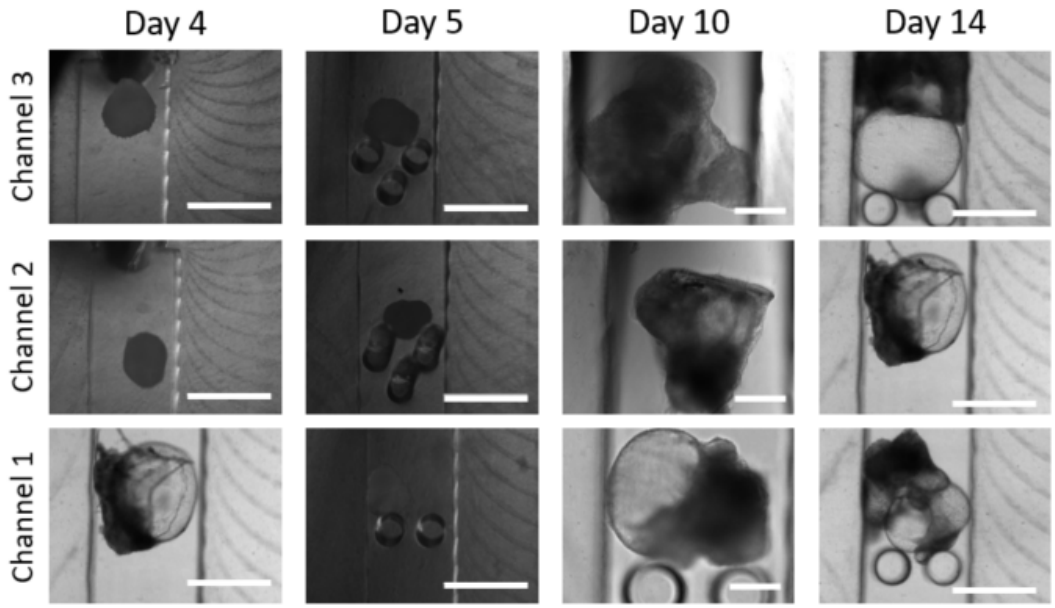


FIGURE 3.9: EBs cultured in larger trapping system. 1) represents an EB in a channel with two pillars and 2,3) represents an EB in a channel with three pillars. Scale bar: 1000 $\mu$m.

When comparing the dead volume present in this chip design and the previous chip design, it is expected that the first design has more dead ends. In both designs there may be parts of the channel and chamber where the flow rate is probably so low that it is likely that the medium is not refreshed in some places. For example, all the corners might have dead volumes where there is almost no flow rate. Those dead ends in the chip designs might form small changes in the differentiation protocol and therefore affect the differentiation effenciency.

Medium in a wells plate is also not fully replaced, since you have to pipette really carefully and have to let the pipette tip rest on the wall inside the well to make sure that the EB is not touched. Thereby, cells also secrete their own factors which can play a role in differentiation [78]. Accurate spatiotemporal control of the soluble microenvironment around cells is a critical aspect for hPSCs differentiation. Thus, it is important that all growth factors are removed carefully while the microenvironment is still controlled.

### 3.4.3 Channel with micro-mechanical valve trap

To prevent the trapping problems of the previous design, a chip without pillars was designed. For this design the same rectangular shaped channels (10x1x1 mm) was used. To prevent the EB from flowing into the inlet or outlet, an extra layer with valves was added, called control layer. Normally, this principle works for closing off rounded channels. In this design the channels are square in cross-section, which would result in half closed channels. The idea behind this is that this would work in such a way that the valves stay closed while the EB is trapped (cannot pass the small area) and medium can still be refreshed.

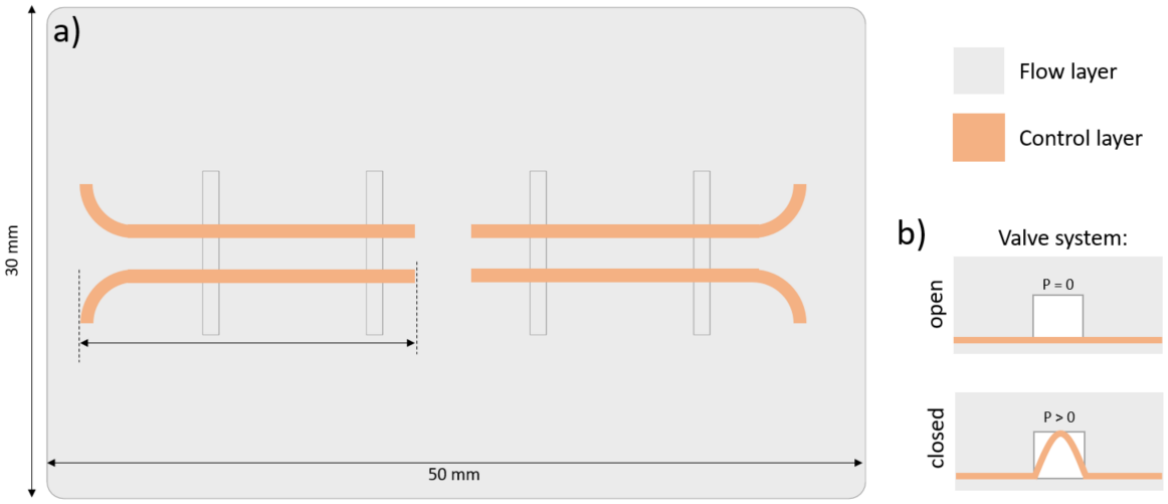


FIGURE 3.10: a) Chip design using micro-mechanical valves. This chip consists of two layers, a flow layer and a control layer. b) Schematic representation of the working principle of the valve.

#### 3.4.3.1 Valve characterization

This final design has a new principle which was tested and evaluated using food coloring. First, the fabrication protocol was optimized for closure of the valves. The closing quality was characterized as good when the channel was half obstructed by the valve.

At first, the relationship between the spin coat speed and flow layer thickness was deviating from previously found results [79]. A thicker membrane is robust and strong, but is consequently less able to deflect which was observed when a membrane of a thinner membrane broke easy (within a few minutes). More membrane thicknesses should be characterized to get more insight into the working mechanism.

For this design, the control layer was spin coated. Characterization of the membrane was performed by creating cross-sections and measuring the thickness of both the membrane and the total thickness of the control layer. Figure 3.11a shows a example of such a cross section and in figure 3.11b a bar graph of the results are shown. It is observed that a spin coat speed of 300 rounds per minute (rpm) for 10 seconds creates a 50 m thick control layer, while the membrane is just 20 $\mu$m thick than with a spin coat speed of 150 rpm for 20 seconds.

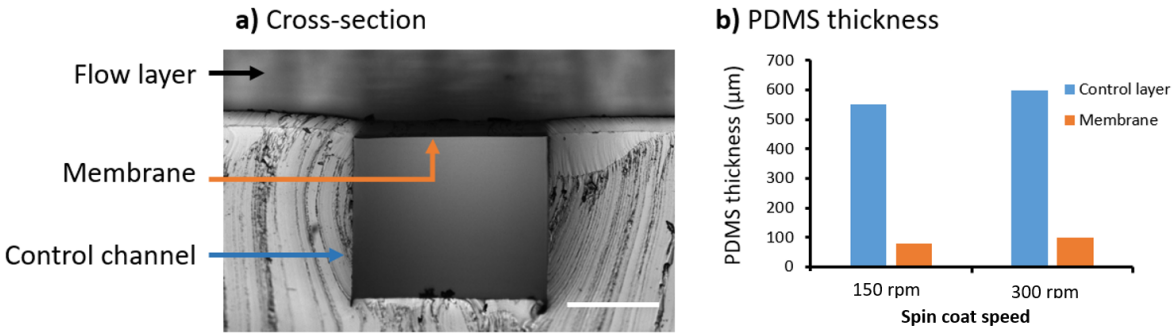


FIGURE 3.11: Cross section measurements of control layer and membrane thickness within the chip with micro-mechanical valves. a) Cross section of the microfluidic chip including a flow channel, a control channel and in between the thin membrane. b) Measured PDMS thickness, where the control layer was fabricated with different spin coat speeds. (n=2)

#### 3.4.3.2 Cell culture in chip using micro-mechanical valves

Once more, EBs were seeded and cultured within the new design from day one as a proof-of-concept experiment. Although this design looked promising and valves were working after optimization, the same problems arose as with the previous design. The valves do not trap the EB and thus the EB is floating around in the chip.

# 4 | Conclusion

In conclusion, several requirements were defined towards asymmetric differentiation on a chip. First of all, the student LAF is the ML-1 lab is not suited for hPSC differentiation to cardiomyocytes, whereas the working environment and pipettes in the Bio imaging center is. The next requirement was to characterise the EB size over time using different initial cell seeding densities. It is not possible to downscale the EB size when the goal is to obtain an appropriate atrial population. EB grows to be up to around 1 mm, therefore the microfluidic chip should at least have a diameter of 1 mm. Channels could be around 500 $\mu$m if the EB does not have to be removed after 14 days of culture to perform flow cytometry analysis because the EBs are still around 400 $\mu$m at day 0. A mixed population of both AMs and VMs is obtained with 0.5 and 1 $\mu$M BMS. To differentiate an EB in a gradient on a chip this means that the steep gradient should obtain those concentrations. A particular challenge was designing a trapping system because of limitations with micro-milling. The trapping systems shown here partially worked for hPSCs differentiation towards VMs as could be seen by the proof-of-concept. One thing to keep in mind is that on chip the volume is (mostly) smaller than in a wells plate. This can influence the behaviour of the micro-environment.

All in all, some requirements were defined for differentiation of hPSCs derived EBs towards asymmetric differentiation of AMs and VMs in a microfluidic system. For the future, those requirements can be used to design a platform that is able to better mimic and study embryogenesis.

# 5 | Future outlook

This chapter presents and explains the future outlook for a new design and parallelization.

## 5.1 New design towards diffusion-based gradients

To be able to asymmetrically differentiate both AMs and VMs in one EB, a steep gradient of BMS should be created. Such a gradient is a natural process that cells use to differentiate and or transmit signals [80]. For future research, a new chip that create and maintain a steep-gradient is presented. The design is based on the pillar inspired microfluidic trapping system and shown in figure A.4. The chip consists of a single unit that should be able to create a gradient due to the small spacing between the pillars. A gradient is easily created by diffusion of proteins from high to low concentrations if the source and sink are maintained at constant concentrations [52].

In order to avoid flow through the chamber by a pressure difference between the two supporting channels, valves could be placed at the cells inlet and outlet. The steady state gradient profile depends on the length of the chamber, the diffusion coefficient, the decay rate and the concentrations of the sink and the source [51, 52].

Previous systems were made out of PDMS because this material is easy in use, biocompatible, oxygen permeable, and flexible, which makes it possible to use the polymer as a cell culture substrate. It is important to notice that PDMS absorbs hydrophobic drugs due to its hydrophobic properties [81]. Most previous 3D cell cultivation platforms that used PDMS observed complications in interpretation of both long-term and short-term drug screening studies [7, 24, 68, 82–84]. BMS-753 is a monobasic aromatic acid, moderately strong, very soluble in alcohol, ether, and benzene, but poorly soluble in water and thus hydrophobic [85]. This means that BMS-753 may be absorbed in PDMS and should be taken into account for choosing a material for this new design. For generating a BMS gradient in a PDMS chip, it means that the gradient might be different than the theoretical gradient.

As was shown in the first design, small dimensions have more advantage in trapping an EB. Besides that, small spacing between pillars results in high hydraulic resistance which than results in no convection. This results in only diffusion. Smaller dimensions (in the range of 10 $\mu$m) are difficult to fabricate with micro-milling.

One of the reasons for choosing micro-milling as a fabrication method in this research is because photolithography requires a high level of practical experience, controlled handling of the substrate, and the use of cleanroom facilities. As a consequence, photolithography is time-consuming, expensive, and labor-intensive, which form the major drawbacks [86]. Instead, micro-milling allows a lot of flexibility and rapid prototyping. Especially, in this early stage of the project it allows for fast and small changes in the design. However, a great advantage of photolithography is that it enables the fabrication of a highly dense network of substantially small dimensions with either sharp edges or half-rounded channels.

It should be taken into account that photolithography is used for smaller structures and consequently smaller heights. Usually channels are only between 50 $\mu$m and 100 $\mu$m high. Although it is possible to make structures up to 500 $\mu$m high. Therefore, it might be an option to fabricate this design with multiple techniques and materials.

## 5.2 High-throughput and parallelization of microfluidic systems

Parallelization can go up to more than a thousand chambers which all can be independently addressed. Another master student, S. de Winter, designed a 16-chamber and 32-chamber parallelized and modular microfluidic chip [87]. In this chip the cell culture compartments are decoupled from the flow layer design, resulting in a modular assembly of three distinct layers: a control, flow and rapid prototype layer (RPT) layer, which is closed off by a substrate such as PDMS or glass. The final microfluidic chip is able to combine small and highly dense mLSI of valves for fluid routing with larger and customized cell culture compartments, so the automated microfluidic chip can be redesigned and utilized for many different OoC applications.

However, the flow layer channels are only 50 $\mu$m high, which is too small for an EB to fit through. A similar upscaled design might work instead. Looking at own designs, it may be possible to integrate the channel shaped chambers into the parallelized chip. For this, a new mold should be created with either 16 or 32 chambers using micro-milling. The RPT layer is fabricated by a combination of casting and injection-molding of PDMS into a micro-milled mold.

Further improving the channel design by changing the trapping mechanism with small changes could lead to a higher trapping success-rate. Instead of pillars, narrowing of the channel at the place of the pillars or integrating other micro-mechanical valves could optimize the design. For parallelization, the total size of the modular chip and the dimensions of the inlets and outlets of the control and flow layers should meet the standard defined ISO values (ISO22916) [88]. This can affect the gradient, since the dimensions are fixated. The way it affects the gradient should be further investigated. Afterwards, new proof-of-concept cell culture for the channel design should be performed. If this works, the channel design can be integrated into the parallelized and modular microfluidic chip.

## 5.3 Automation of microfluidic systems

To allow control over the experiments both design ideas can be controlled either manually or through predefined programs using a custom LabVIEW program [52, 61]. This program allows automation of PDMS coating, cells seeding, gradient generation, imaging and cleaning. Coupled with an automated microscope, this could automate many experiments in parallel to increase the throughput of cell-biological measurements.

## 5.4 In-air cell encapsulation

Another approach to form an EB on chip is in-air cell encapsulation. Encapsulation is a specific form of compartmentalization where cells are confined within a micromaterial such as a microgel or microfiber. In-air microfluidics are biocompatible, for 3D modular constructs with tailored microenvironments for multiple cell types [89].

Schot et al. stated that encapsulation using continuous microfluidics provides an ideal balance between scalability and uniformity [90]. Thereby, it is able to expand cells into larger quantities and/or more complex modalities.

Traditional methods to produce microtissues rely on the culture in microwells and other techniques, leading to low uniformity due to fusion and low throughput. By compartmentalizing cells in microcapsules using high-throughput microfluidics, microtissues can be produced in large quantities while maintaining microtissue uniformity. When comparing microwells to in-air cell encapsulation, there is one important difference [90]. Microwells can only be used for monodisperse tissues, while in-air cell encapsulation can be done with polydisperse tissues. Both can form tissues of up to 1 mm in diameter. However, cleaner, faster, and more scalable microfluidic processes need to be developed to actually use this type of technique for asymmetric differentiation.

# Bibliography


1. Roth, G. A. *et al.* Global Burden of Cardiovascular Diseases and Risk Factors, 1990–2019: Update From the GBD 2019 Study. *Journal of the American College of Cardiology* **76,** 2982–3021. ISSN: 0735-1097 (Dec. 2020).
2. Virani, S. S. *et al.* Heart Disease and Stroke Statistics - 2021 Update: A Report From the American Heart Association. *Circulation* **143,** E254–E743. ISSN: 15244539 (Feb. 2021).
3. Thomas, H. *et al.* Global Atlas of Cardiovascular Disease 2000-2016: The Path to Prevention and Control. *Global heart* **13,** 143–163. ISSN: 2211-8179 (Sept. 2018).
4. Carlson, B. M. Embryology in the medical curriculum. *The Anatomical Record* **269,** 89–98. ISSN: 1097-0185 (Apr. 2002).
5. Slaats, R. H. *Modelling the human heart: Human stem cell-based models lead the way in physiological, pathological, and toxicological research* tech. rep. (University of Twente, Enschede, The Netherlands, 2021), 183.
6. *The cardiovascular system: the heart, Cardiac Muscle and Electrical Activity* 783–832. ISBN: 978-1-938168-13-0 (OpenStax College, Rice University, Houston, Texas, 2013).
7. Mathur, A. *et al.* Human iPSC-based Cardiac Microphysiological System For Drug Screening Applications. *Scientific Reports* **5,** 1–7. ISSN: 2045-2322 (Mar. 2015).
8. Bhatia, S. N. & Ingber, D. E. Microfluidic organs-on-chips. *Nature Biotechnology* **32,** 760–772. ISSN: 1546-1696 (2014).
9. Khoruzhenko, A. I. 2D- and 3D-cell culture. *Biopolymers and Cell* **27,** 17–24. ISSN: 19936842 (2011).
10. Asthana, A. & Kisaalita, W. S. Biophysical microenvironment and 3D culture physiological relevance. *Drug discovery today* **18,** 533–540. ISSN: 1878-5832 (2013).
11. Van Duinen, V., Trietsch, S. J., Joore, J., Vulto, P. & Hankemeier, T. Microfluidic 3D cell culture: from tools to tissue models. *Current opinion in biotechnology* **35,** 118–126. ISSN: 1879-0429 (2015).
12. Beqqali, A., Van Eldik, W., Mummery, C. & Passier, R. Human stem cells as a model for cardiac differentiation and disease. *Cellular and Molecular Life Sciences 2009 66:5* **66,** 800–813. ISSN: 1420-9071 (Jan. 2009).
13. Braam, S. R. *et al.* Prediction of drug-induced cardiotoxicity using human embryonic stem cell-derived cardiomyocytes. *Stem cell research* **4,** 107–116. ISSN: 1876-7753. `https://pubmed.ncbi.nlm.nih.gov/20034863/` (Mar. 2010).
14. Devalla, H. D. *et al.* Atrial-like cardiomyocytes from human pluripotent stem cells are a robust preclinical model for assessing atrial-selective pharmacology. *EMBO Molecular Medicine* **7,** 394–410. ISSN: 1757-4684 (Apr. 2015).

15. Van Meer, B. J., Tertoolen, L. G. & Mummery, C. L. Concise Review: Measuring Physiological Responses of Human Pluripotent Stem Cell Derived Cardiomyocytes to Drugs and Disease. *Stem cells (Dayton, Ohio)* **34,** 2008–2015. ISSN: 1549-4918 (Aug. 2016).

16. Sala, L., Bellin, M. & Mummery, C. L. Integrating cardiomyocytes from human pluripotent stem cells in safety pharmacology: has the time come? *British journal of pharmacology* **174,** 3749–3765. ISSN: 1476-5381 (Nov. 2017).

17. Giacomelli, E., Mummery, C. L. & Bellin, M. Human heart disease: lessons from human pluripotent stem cell-derived cardiomyocytes. *Cellular and molecular life sciences : CMLS* **74,** 3711–3739. ISSN: 1420-9071 (Oct. 2017).

18. Ahn, S. *et al.* Mussel-inspired 3D Fiber Scaffolds for Heart-on-a-Chip Toxicity Studies of Engineered Nanomaterials. *Analytical and bioanalytical chemistry* **410,** 6141. ISSN: 16182650 (Sept. 2018).

19. Eschenhagen, T., Eder, A., Vollert, I. & Hansen, A. Physiological aspects of cardiac tissue engineering. *American journal of physiology. Heart and circulatory physiology* **303.** ISSN: 1522-1539 (July 2012).

20. Lemoine, M. D. *et al.* Human iPSC-derived cardiomyocytes cultured in 3D engineered heart tissue show physiological upstroke velocity and sodium current density. *Scientific Reports* **7.** ISSN: 20452322 (Dec. 2017).

21. Lind, J. U. *et al.* Instrumented cardiac microphysiological devices via multi-material 3D printing. *Nature materials* **16,** 303. ISSN: 14764660 (Mar. 2017).

22. Lind, J. U. *et al.* Cardiac Microphysiological Devices with Flexible Thin-Film Sensors for Higher-Throughput Drug Screening. *Lab on a chip* **17,** 3692. ISSN: 14730189 (Oct. 2017).

23. Macqueen, L. A. *et al.* A tissue-engineered scale model of the heart ventricle. *Nature Biomedical Engineering 2018 2:12* **2,** 930–941. ISSN: 2157-846X (July 2018).

24. Nunes, S. S. *et al.* Biowire: a new platform for maturation of human pluripotent stem cell derived cardiomyocytes. *Nature methods* **10,** 781. ISSN: 15487091 (Aug. 2013).

25. Schaaf, S. *et al.* Human Engineered Heart Tissue as a Versatile Tool in Basic Research and Preclinical Toxicology. *PLoS ONE* **6,** 26397. ISSN: 19326203 (2011).

26. Tulloch, N. L. *et al.* Growth of Engineered Human Myocardium with Mechanical Loading and Vascular Co-culture. *Circulation research* **109,** 47. ISSN: 00097330 (June 2011).

27. Lemoine, M. D. *et al.* Human Induced Pluripotent Stem Cell-Derived Engineered Heart Tissue as a Sensitive Test System for QT Prolongation and Arrhythmic Triggers. *Circulation. Arrhythmia and electrophysiology* **11.** ISSN: 1941-3084 (July 2018).

28. Tiburcy, M. *et al.* Defined Engineered Human Myocardium with Advanced Maturation for Applications in Heart Failure Modelling and Repair. *Circulation* **135,** 1832. ISSN: 15244539 (May 2017).

29. Goldfracht, I. *et al.* Generating ring-shaped engineered heart tissues from ventricular and atrial human pluripotent stem cell-derived cardiomyocytes. *Nature Communications 2020 11:1* **11,** 1–15. ISSN: 2041-1723 (Jan. 2020).

30. Pei, F. *et al.* Chemical-defined and albumin-free generation of human atrial and ventricular myocytes from human pluripotent stem cells. *Stem cell research* **19,** 94–103. ISSN: 1876-7753 (Mar. 2017).

31. Schwach, V. *et al.* A COUP-TFII Human Embryonic Stem Cell Reporter Line to Identify and Select Atrial Cardiomyocytes. *Stem cell reports* **9,** 1765–1779. ISSN: 2213-6711 (2017).

32. Lee, J. H., Protze, S. I., Laksman, Z., Backx, P. H. & Keller, G. M. Human Pluripotent Stem Cell-Derived Atrial and Ventricular Cardiomyocytes Develop from Distinct Mesoderm Populations. *Cell stem cell* **21,** 179–194. ISSN: 1875-9777 (Aug. 2017).
33. Schwach, V., Cofiño-Fabres, C., ten Den, S. A. & Passier, R. Improved Atrial Differentiation of Human Pluripotent Stem Cells by Activation of Retinoic Acid Receptor Alpha (RAR$\alpha$). *Journal of Personalized Medicine* **12,** 628. ISSN: 2075-4426 (Apr. 2022).
34. Van Der Hooft, C. S. *et al.* Drug-induced atrial fibrillation. *Journal of the American College of Cardiology* **44,** 2117–2124. ISSN: 0735-1097 (Dec. 2004).
35. Chen, L. Y. *et al.* Atrial Fibrillation and the Risk of Sudden Cardiac Death: The Atherosclerosis Risk in Communities (ARIC) Study and Cardiovascular Health Study (CHS). *JAMA internal medicine* **173,** 29. ISSN: 21686106 (Jan. 2013).
36. Eisen, A. *et al.* Sudden Cardiac Death in Patients With Atrial Fibrillation: Insights From the ENGAGE AF-TIMI 48 Trial. *Journal of the American Heart Association: Cardiovascular and Cerebrovascular Disease* **5.** ISSN: 20479980 (July 2016).
37. Dobrev, D. & Nattel, S. New antiarrhythmic drugs for treatment of atrial fibrillation. *The Lancet* **375,** 1212–1223. ISSN: 0140-6736 (Apr. 2010).
38. Schwach, V., Slaats, R. H. & Passier, R. Human Pluripotent Stem Cell-Derived Cardiomyocytes for Assessment of Anticancer Drug-Induced Cardiotoxicity. *Frontiers in Cardiovascular Medicine* **7,** 50. ISSN: 2297055X (Apr. 2020).
39. Honda, Y., Li, J., Hino, A., Tsujimoto, S. & Lee, J. K. High-Throughput Drug Screening System Based on Human Induced Pluripotent Stem Cell-Derived Atrial Myocytes A Novel Platform to Detect Cardiac Toxicity for Atrial Arrhythmias. *Frontiers in Pharmacology* **12,** 1917. ISSN: 16639812 (Aug. 2021).
40. Keegan, B. R., Meyer, D. & Yelon, D. Organization of cardiac chamber progenitors in the zebrafish blastula. *Development (Cambridge, England)* **131,** 3081–3091. ISSN: 0950-1991 (July 2004).
41. Zhang, Q. *et al.* Direct differentiation of atrial and ventricular myocytes from human embryonic stem cells by alternating retinoid signals. *Cell research* **21,** 579–587. ISSN: 1748-7838 (Apr. 2011).
42. Devalla, H. D. *et al.* Atrial-like cardiomyocytes from human pluripotent stem cells are a robust preclinical model for assessing atrial-selective pharmacology. *EMBO Molecular Medicine* **7,** 394–410. ISSN: 1757-4684 (2015).
43. Abi-Gerges, N., Miller, P. E. & Ghetti, A. Human Heart Cardiomyocytes in Drug Discovery and Research: New Opportunities in Translational Sciences. *Current pharmaceutical biotechnology* **21,** 787–806. ISSN: 1873-4316 (Dec. 2020).
44. Gharanei, M. *et al.* Atrial-specific hiPSC-derived cardiomyocytes in drug discovery and disease modeling. *Methods (San Diego, Calif.)* **203,** 364–377. ISSN: 1095-9130 (July 2022).
45. Grandi, E. *et al.* Human Atrial Action Potential and Ca2+ Model: Sinus Rhythm and Chronic Atrial Fibrillation. *Circulation research* **109,** 1055. ISSN: 00097330 (Oct. 2011).
46. Vidarsson, H., Hyllner, J. & Sartipy, P. Differentiation of human embryonic stem cells to cardiomyocytes for in vitro and in vivo applications. *Stem cell reviews and reports* **6,** 108–120. ISSN: 2629-3277 (2010).
47. Murke, F., Da Conceição Castro, S. V., Giebel, B. & Görgens, A. Concise Review: Asymmetric Cell Divisions in Stem Cell Biology. *Symmetry 2015, Vol. 7, Pages 2025-2037* **7,** 2025–2037. ISSN: 20738994 (Nov. 2015).

48. Knoblich, J. A. Mechanisms of Asymmetric Stem Cell Division. *Cell* **132,** 583–597. ISSN: 00928674 (2008).

49. Chhabra, S. N. & Booth, B. W. Asymmetric cell division of mammary stem cells. *Cell Division* **16,** 1–15. ISSN: 17471028 (2021).

50. Wartlick, O., Kicheva, A. & González-Gaitán, M. Morphogen Gradient Formation. *Cold Spring Harbor Perspectives in Biology* **1.** ISSN: 19430264 (2009).

51. Cooksey, G. A., Sip, C. G. & Folch, A. A multi-purpose microfluidic perfusion system with combinatorial choice of inputs, mixtures, gradient patterns, and flow rates. *Lab on a chip* **9,** 417–426. ISSN: 14730189 (2009).

52. Frank, T. & Tay, S. Flow-switching allows independently programmable, extremely stable, high-throughput diffusion-based gradients. *Lab on a Chip* **13,** 1273–1281. ISSN: 1473-0189 (Mar. 2013).

53. Carvalho, V. *et al.* The Effect of Dynamic, In Vivo-like Oxaliplatin on HCT116 Spheroids in a Cancer-on-Chip Model Is Representative of the Response in Xenografts. *Micromachines* **13** (2022).

54. Wu, M. H., Huang, S. B., Cui, Z., Cui, Z. & Lee, G. B. A high throughput perfusion-based microbioreactor platform integrated with pneumatic micropumps for three dimensional cell culture. *Biomedical Microdevices* **10,** 309–319. ISSN: 13872176 (Apr. 2008).

55. Wu, L. Y., Di Carlo, D. & Lee, L. P. Microfluidic self-assembly of tumor spheroids for anticancer drug discovery. *Biomedical Microdevices* **10,** 197–202. ISSN: 13872176 (Apr. 2008).

56. Skelley, A. M., Kirak, O., Suh, H., Jaenisch, R. & Voldman, J. Microfluidic Control of Cell Pairing and Fusion. *Nature methods* **6,** 147. ISSN: 15487091 (2009).

57. Palacio-Castañeda, V., Velthuijs, N., Le Gac, S. & Verdurmen, W. P. Oxygen control: the often overlooked but essential piece to create better in vitro systems. *Lab on a Chip* **22,** 1068–1092. ISSN: 14730189 (Mar. 2022).

58. Khoury, M. *et al.* A microfluidic traps system supporting prolonged culture of human embryonic stem cells aggregates. *Biomedical microdevices* **12,** 1001–1008. ISSN: 1572-8781 (2010).

59. Luan, Q., Macaraniag, C., Zhou, J. & Papautsky, I. Microfluidic systems for hydrodynamic trapping of cells and clusters. *Biomicrofluidics* **14,** 031502. ISSN: 19321058 (2020).

60. Vollertsen, A. R. *et al.* Modular operation of microfluidic chips for highly parallelized cell culture and liquid dosing via a fluidic circuit board. *Microsystems & Nanoengineering* **6,** 1–16. ISSN: 2055-7434 (2020).

61. Vollertsen, A. R. *et al.* Highly parallelized human embryonic stem cell differentiation to cardiac mesoderm in nanoliter chambers on a microfluidic chip. *Biomedical Microdevices* **23,** 30. ISSN: 15728781 (2021).

62. Ardila Riveros, J. C. *et al.* Automated optimization of endoderm differentiation on chip. *Lab on a Chip* **21,** 4685–4695. ISSN: 1473-0189 (2021).

63. Zhao, Y. *et al.* A Platform for Generation of Chamber-Specific Cardiac Tissues and Disease Modeling. *Cell* **176,** 913–927. ISSN: 1097-4172 (Feb. 2019).

64. Grosberg, A., Alford, P. W., McCain, M. L. & Parker, K. K. Ensembles of engineered cardiac tissues for physiological and pharmacological study: Heart on a chip. *Lab on a Chip* **11,** 4165–4173. ISSN: 1473-0189 (2011).

65. Ribas, J. *et al.* Cardiovascular Organ-on-a-Chip Platforms for Drug Discovery and Development. *Applied in Vitro Toxicology* **2,** 82–96. ISSN: 2332-1512 (2016).

66. Ma, Q., Ma, H., Xu, F., Wang, X. & Sun, W. Microfluidics in cardiovascular disease research: state of the art and future outlook. *Microsystems & Nanoengineering 2021 7:1* **7,** 1–19. ISSN: 2055-7434 (2021).

67. Ribeiro, M. C. *et al.* A New Versatile Platform for Assessment of Improved Cardiac Performance in Human-Engineered Heart Tissues. *Journal of Personalized Medicine 2022, Vol. 12, Page 214* **12,** 214. ISSN: 2075-4426 (Feb. 2022).

68. Sidorov, V. Y. *et al.* I-Wire Heart-on-a-Chip I: Three-dimensional cardiac tissue constructs for physiology and pharmacology. *Acta biomaterialia* **48,** 68. ISSN: 18787568 (Jan. 2017).

69. Abulaiti, M. *et al.* Establishment of a heart-on-a-chip microdevice based on human iPS cells for the evaluation of human heart tissue function. *Scientific Reports 2020 10:1* **10,** 1–12. ISSN: 2045-2322 (Nov. 2020).

70. Liu, J. C., Lerou, P. H. & Lahav, G. Stem cells: balancing resistance and sensitivity to DNA damage. *Trends in Cell Biology* **24,** 268–274. ISSN: 0962-8924 (May 2014).

71. Dumitru, R. *et al.* Human Embryonic Stem Cells Have Constitutively Active Bax at the Golgi and Are Primed to Undergo Rapid Apoptosis. *Molecular Cell* **46,** 573–583. ISSN: 10972765 (June 2012).

72. Liu, J. C. *et al.* High mitochondrial priming sensitizes hESCs to DNA-damage-induced apoptosis. *Cell Stem Cell* **13,** 483–491. ISSN: 18759777 (Oct. 2013).

73. Birket, M. J. *et al.* Contractile Defect Caused by Mutation in MYBPC3 Revealed under Conditions Optimized for Human PSC-Cardiomyocyte Function. *Cell reports* **13,** 733–745. ISSN: 2211-1247 (Oct. 2015).

74. Cumming, G., Fidler, F. & Vaux, D. L. Error bars in experimental biology. *Journal of Cell Biology* **177,** 7–11. ISSN: 0021-9525 (Apr. 2007).

75. Almarza, A. J. & Athanasiou, K. A. Effects of Initial Cell Seeding Density for the Tissue Engineering of the Temporomandibular Joint Disc. *Annals of Biomedical Engineering 2005 33:7* **33,** 943–950. ISSN: 1573-9686 (July 2005).

76. Wang, L., Sheshareddy, K., Weiss, M. L. & Detamore, M. S. Effect of initial seeding density on human umbilical cord mesenchymal stromal cells for fibrocartilage tissue engineering. *Tissue Engineering - Part A* **15,** 1009–1017. ISSN: 1937335X (May 2009).

77. Najafabadi, M. M., Bayati, V., Orazizadeh, M., Hashemitabar, M. & Absalan, F. Impact of Cell Density on Differentiation Efficiency of Rat Adipose-derived Stem Cells into Schwann-like Cells. *International Journal of Stem Cells* **9,** 213. ISSN: 20055447 (2016).

78. Giobbe, G. G. *et al.* Functional differentiation of human pluripotent stem cells on a chip. *Nature Methods 2015 12:7* **12,** 637–640. ISSN: 1548-7105. `https://www.nature.com/articles/nmeth.3411` (June 2015).

79. Rho, H. S. *Proteins on a chip* PhD thesis (University of Twente, Enschede, The Netherlands, Apr. 2016). ISBN: 9789036540926.

80. Lander, A. D. Morpheus Unbound: Reimagining the Morphogen Gradient. *Cell* **128,** 245–256. ISSN: 00928674 (Jan. 2007).

81. Toepke, M. W. & Beebe, D. J. PDMS absorption of small molecules and consequences in microfluidic applications. *Lab on a chip* **6,** 1484–1486. ISSN: 1473-0197 (2006).

82. Huebsch, N. *et al.* Miniaturized iPS-Cell-Derived Cardiac Muscles for Physiologically Relevant Drug Response Analyses. *Scientific Reports* **6.** ISSN: 20452322 (Apr. 2016).

83. Wang, G. *et al.* Modeling the mitochondrial cardiomyopathy of Barth syndrome with iPSC and heart-on-chip technologies. *Nature medicine* **20,** 616. ISSN: 1546170X (2014).

84. Hinson, J. T. *et al.* Titin Mutations in iPS cells Define Sarcomere Insufficiency as a Cause of Dilated Cardiomyopathy. *Science (New York, N.Y.)* **349,** 982. ISSN: 10959203 (Aug. 2015).

85. Géhin, M. *et al.* Structural basis for engineering of retinoic acid receptor isotype-selective agonists and antagonists. *Chemistry and Biology* **6.** ISSN: 10745521 (1999).

86. Rodrigo Martinez-Duarte and Marc J. Madou. in *Microfluidics and Nanofluidics Handbook* (ed Sushanta K. Mitra, S. C.) 231–268 (CRC Press, 2011). ISBN: 9780429093371.

87. S. de Winter. *Modular and automated parallelization of organ-on-chip technology; Using rapid prototyping towards numerous design possibilities* Enschede, 2022.

88. *ISO - ISO 22916:2022 - Microfluidic devices — Interoperability requirements for dimensions, connections and initial device classification* 2022. `https://www.iso.org/standard/74157.html`.

89. Visser, C. W., Kamperman, T., Karbaat, L. P., Lohse, D. & Karperien, M. In-air microfluidics enables rapid fabrication of emulsions, suspensions, and 3D modular (bio)materials. *Science Advances* **4.** ISSN: 23752548 (Jan. 2018).

90. Schot, M., Araújo-Gomes, N., van Loo, B., Kamperman, T. & Leijten, J. Scalable fabrication, compartmentalization and applications of living microtissues. *Bioactive materials* **19,** 392–405. ISSN: 2452-199X (Apr. 2022).

# A Appendix

This chapter shows additional information or raw data that supports the main document or report.

## A.1 Overview of the best FACS results

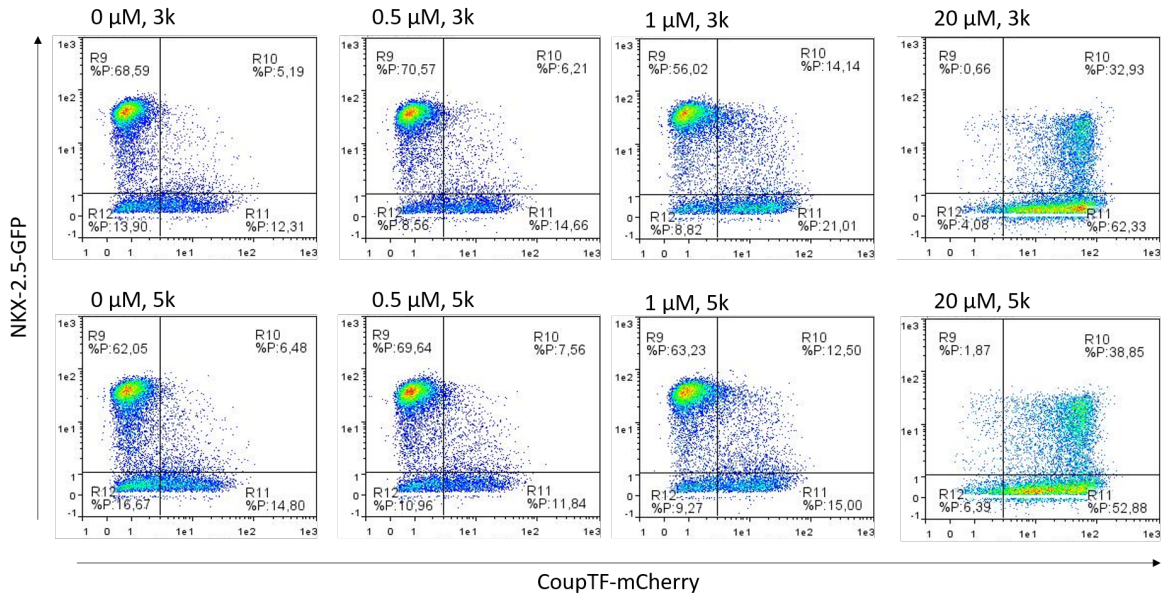


FIGURE A.1: FACS graphs with the highest percentages AMs and VMs. Replication of the RAR$\alpha$ induced protocol in the BIC using 3k and 5k cell seeding density and concentrations of 0, 0.5, 1 and 20 $\mu$M BMS.

## A.2 FACS result of inexperienced researcher compared to experienced researcher

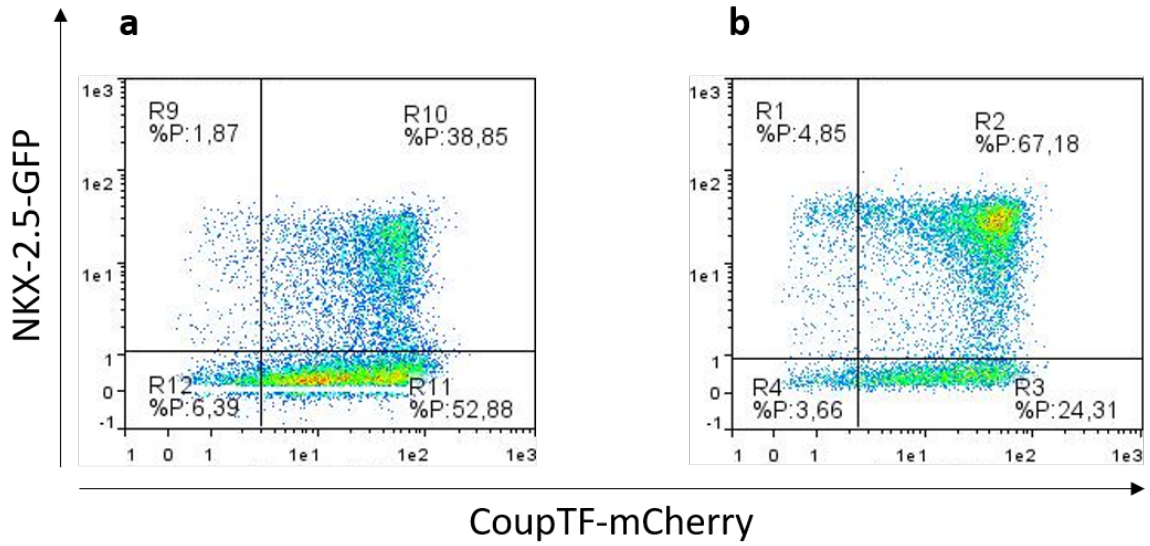


FIGURE A.2: FACS graphs of the same stem cell passage number a) from the inexperienced stem cell researcher and b) from the experienced stem cell researcher. Both are performed in the BIC 5k cell seeding density and 20 $\mu$M BMS.

## A.3 Raw data characterization of micromilled system

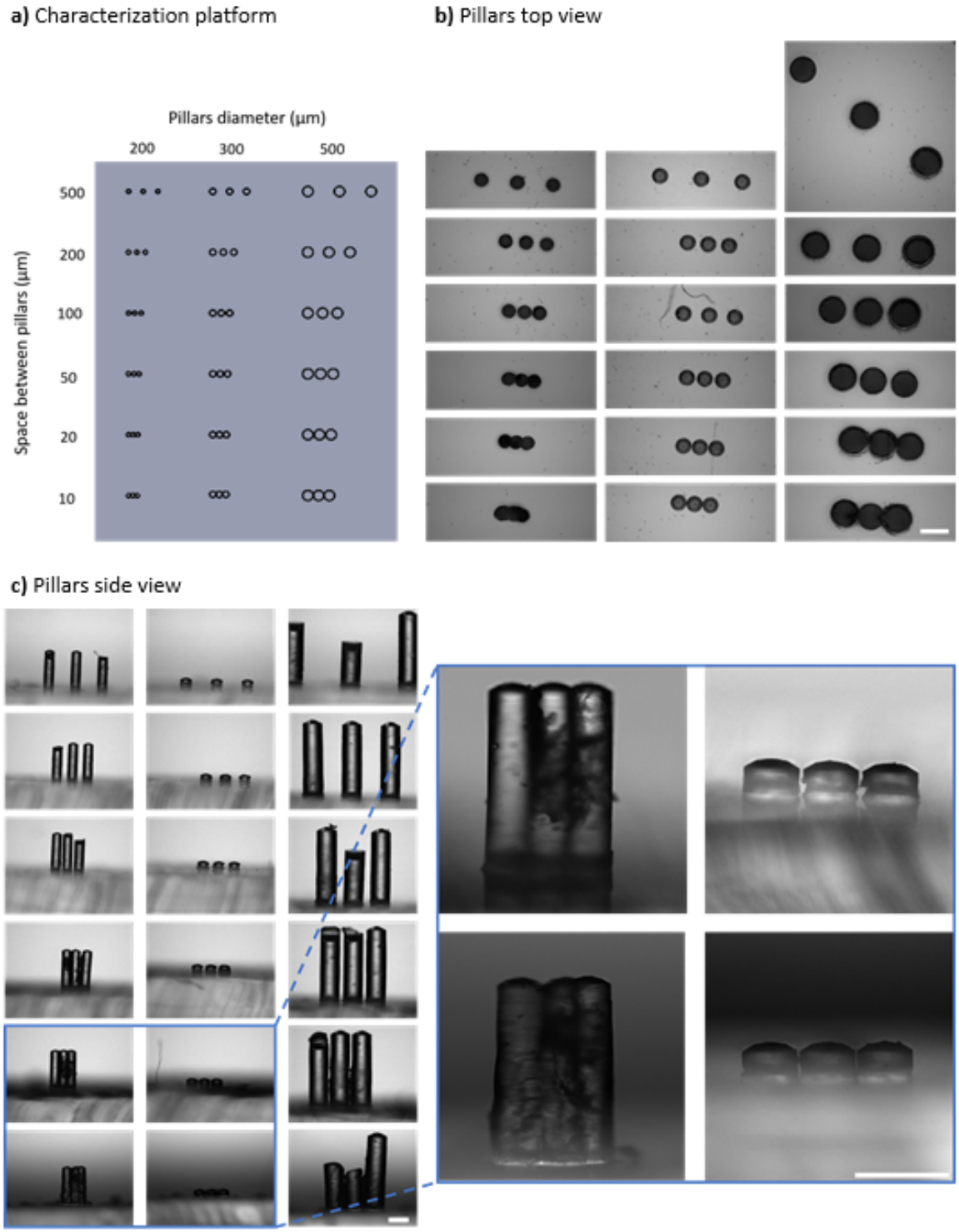


FIGURE A.3: Characterization platform (a), top view results of the milled platform (b), and side view results of the fabricated PDMS pillars (c). PDMS pillars with 300 $\mu$m and small space in between (10 or 20 $\mu$m) are separate, while 200 $\mu$m with small spacing are not. Scale bars: 500 $\mu$m.

## A.4 Future concept design

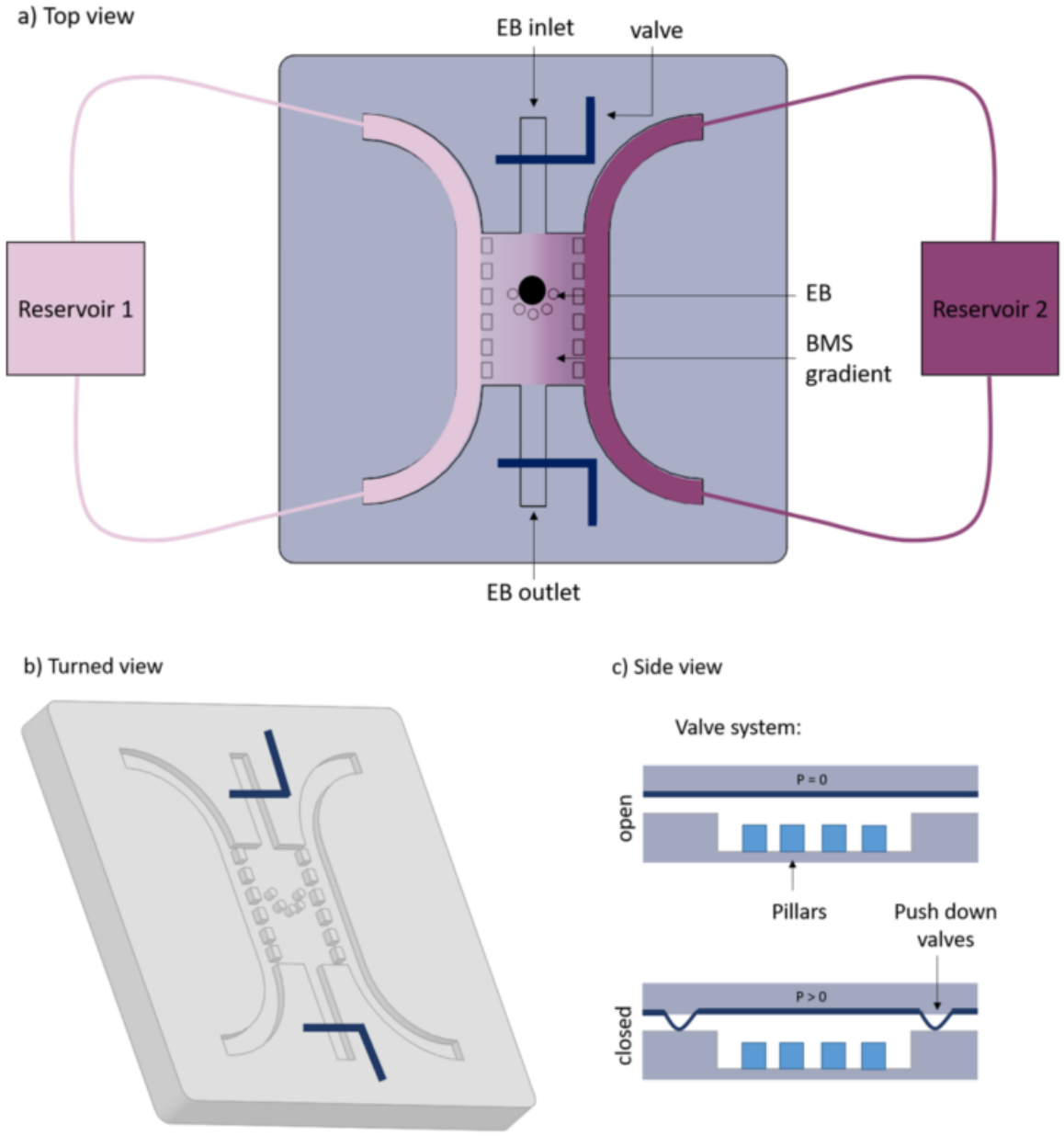


FIGURE A.4: Concept design of a future chip design with reservoirs for recirculating medium consisting of a low BMS concentration in reservoir 1 and a high BMS concentration in reservoir 2 to create a steep gradient. Pillars should create a diffusion-based gradient, rounded pillars for trapping an EB, and valves to open and close access to the inlet and outlet. a) Top view of assembled chip with control and flow layer, an EB, tubing and reservoirs, b) turned view, and c) the side view of the working principle of the push down valves. Not on scale.